Western North Pacific tropical cyclone model tracks in present and future climates

Jennifer Nakamura,[1] Suzana J. Camargo,[1] Adam H. Sobel,[1,2] Naomi Henderson,[1] Kerry A. Emanuel,[3] Arun Kumar,[4] Timothy E. LaRow,[5] Hiroyuki Murakami,[6] Malcolm J. Roberts,[7] Enrico Scoccimarro,[8,9] Pier Luigi Vidale,[10] Hui Wang,[4] Michael F. Wehner,[11] Ming Zhao[6]

Corresponding author: Suzana J. Camargo, Lamont-Doherty Earth Observatory, Columbia University, PO Box 1000, Palisades, NY 10960. (suzana@ldeo.columbia.edu)

[1]Lamont-Doherty Earth Observatory, Columbia University, Palisades, New York, USA.

[2]Department of Applied Physics and Applied Mathematics, Columbia University, New York, New York, USA.

[3]Program in Atmospheres, Oceans and Climate, Massachusetts Institute of Technology, Cambridge, Massachusetts, USA.

This article has been accepted for publication and undergone full peer review but has not been through the copyediting, typesetting, pagination and proofreading process, which may lead to differences between this version and the Version of Record. Please cite this article as doi: 10.1002/2017JD027007

Abstract. Western North Pacific tropical cyclone (TC) model tracks are analyzed in two large multi-model ensembles, spanning a large variety of models and multiple future climate scenarios. Two methodologies are used to synthesize the properties of TC tracks in this large dataset: cluster analysis and mass moments ellipses. First, the models' TC tracks are compared to observed

[4]NOAA/NWS/NCEP Climate Prediction Center, College Park, Maryland, USA.

[5]Verato Inc., McLean, Virginia, USA.

[6]NOAA Geophysical Fluid Dynamics Laboratory, Princeton, New Jersey, USA.

[7]Met Office, Hadley Center, Devon, United Kingdom.

[8]Istituto Nazionale di Geofisica e Vulcanologia (INGV), Bologna, Italy.

[9]Centro Euro-Mediterraneo sui Cambiamenti Climatici (CMCC), Bologna, Italy.

[10]NCAS-Climate, University of Reading, United Kingdom.

[11]Lawrence Berkeley National Laboratory, Berkeley, California, USA.

TC tracks' characteristics and a subset of the models is chosen for analysis, based on the tracks' similarity to observations and sample size. Potential changes in track types in a warming climate are identified by comparing the kernel smoothed probability distributions of various track variables in historical and future scenarios using a Kolmogorov-Smirnov significance test. Two track changes are identified. The first is a statistically significant increase in the North-South expansion, which can also be viewed as a poleward shift, as TC tracks are prevented from expanding equatorward due to the weak Coriolis force near the Equator. The second change is an eastward shift in the storm tracks that occur near the central Pacific in one of the multi-model ensembles, indicating a possible increase in the occurrence of storms near Hawaii in a warming climate. The dependence of the results on which model and future scenario are considered emphasizes the necessity of including multiple models and scenarios when considering future changes in TC characteristics.

Keypoints:

- Western North Pacific tropical cyclone tracks' characteristics in two multi-model datasets are compared with observed tracks.
- The existence of statistically significant and robust changes in tracks under a warming climate is analyzed.
- Two main track changes are identified: (i) a statistically significant northward shift in the most common track type; (ii) an eastward shift in the clus-

ter with tracks that can potentially affect Hawaii in one of the multi-model datasets.

1. Introduction

There is a large body of research aiming to understand how tropical cyclones' (TCs) characteristics are influenced by climate change [*Knutson et al.*, 2010; *Walsh et al.*, 2016]. Most studies have focused on changes in global TC frequency and intensity in a warming climate [*Camargo*, 2013; *Murakami et al.*, 2014; *Knutson et al.*, 2015]. As computational resources have increased and global climate models' ability to simulate TCs has improved [*Camargo and Wing*, 2016], analyses of other aspects of TC characteristics, including regional studies, have gained momentum in the modeling community [*Villarini and Vecchi*, 2012; *Scoccimarro et al.*, 2014; *Dwyer et al.*, 2015].

A TC's landfall location depends on its track. There is large element of inherent randomness (from a climate perspective) in each TC's track, as it is a function of the steering winds, which can be highly variable on a range of time scales. Some tracks can diverge from the historical record, as in the case of Hurricane Sandy [*Hall and Sobel*, 2013]. Nevertheless, climatologically there are typical track types that occur in each TC basin. The possibility that there may be changes in the properties of these typical TC tracks due to climate change is of great interest, due to the possibility of changes in landfall occurrence. However, in order for these projections of track changes to be credible, they need to be statistically significant and robust across a large number of models and climate change scenarios.

We focus here on TC tracks over the western North Pacific (WNP) basin. The WNP, climatologically, is the region with the largest number of TCs per year. Typhoons in the WNP can have large impacts in many Asian countries including the Philippines, China,

Taiwan, Japan, Vietnam and South Korea. A tragic example of the large impacts of a landfalling TC in this region was super-typhoon Haiyan, which devastated the Philippines in 2013 [*Lander et al.*, 2014; *Lin et al.*, 2014].

Over the last several decades, there has been a poleward shift in the average latitude of TC lifetime maximum intensities globally [*Kossin et al.*, 2014]. This shift is very robust in the WNP, and is projected to continue through the end of the century [*Kossin et al.*, 2016]. This poleward shift is expected to cause systematic shifts in the areas at greatest TC risk in the region. On the other hand, *Lin and Chan* [2015] noticed a decrease in the typhoon destructive potential in the Asia Pacific region and linked it to changes in the Pacific subtropical high, which is strongly related to TC tracks. *Mei and Xie* [2016] noticed an increase in the observed intensities of the TCs making landfall in Asia since late 1970s. More recently, *Daloz and Camargo* [2017] found a significant poleward shift in the mean genesis position over the Pacific basins, associated with a poleward shift in the genesis indices in the region. While *Liang et al.* [2017] showed a connected poleward shift in typhoon-induced rainfall over Taiwan.

Currently, there is no clear consensus on the projections of track changes in this region. While in some models there is a poleward (northward in the WNP) shift [*Wu et al.*, 2014], in others there is an eastward shift towards the Central North Pacific [*Li et al.*, 2010; *Murakami et al.*, 2011; *Yokoi et al.*, 2013; *Mori et al.*, 2013], a combination of both [*Zhao and Held*, 2012; *Murakami et al.*, 2012; *Colbert et al.*, 2015; *Roberts et al.*, 2015], or even a southeastward shift [*Manganello et al.*, 2014]. Given these results, it is important to consider a uniform statistical approach across multi-model datasets to this problem, so

that we can investigate the robustness and statistical significance of track changes in the WNP under global warming.

Our analysis here considers the WNP tracks in current and future climates in two multi-model datasets. The first dataset is the U.S. CLIVAR Hurricane Working Group (HWG), with contributions from multiple modeling groups. Each modeling group performed high-resolution (0.25° to 1.25°) global climate model simulations using the same forcings for the current climate, as well as for highly idealized future climate change scenarios. Various aspects of the HWG simulations have been analyzed in the literature, and a summary of these results appeared in *Walsh et al.* [2015]. Of particular interest are the results of *Daloz et al.* [2015], who analyzed the TC tracks over the North Atlantic basin, using a similar methodology as that applied here to the WNP.

The second multi-model dataset considered here is that from the Fifth Coupled Model Intercomparison Project (CMIP5) [*Taylor et al.*, 2012]. Fourteen models were analyzed in the historical and one warming scenario, namely the representative concentration pathway 8.5 (RCP8.5). Most CMIP5 global climate models have low horizontal resolution (1.2° to 3.0°), and the TC activity climatologies in these models have well known biases, such as TC intensities lower than observations [*Camargo*, 2013]. Despite these biases, it is possible to obtain useful information from the TC projections from the CMIP5 models as shown in *Camargo* [2013]; *Tory et al.* [2013]; *Tang and Camargo* [2014] and *Kossin et al.* [2016].

In addition to the TC tracks obtained by detecting tropical cyclone-like features[1] directly in the model output, we also include in our analysis TC synthetic tracks obtained by a statistical-dynamical downscaling methodology [*Emanuel et al.*, 2008] using the large-

scale environmental fields simulated by the models as inputs. Synthetic tracks have been generated using this method for a subset of the models from the HWG [*Daloz et al.*, 2015] and CMIP5 [*Emanuel*, 2013; *Dwyer et al.*, 2015] datasets.

Although there are many papers analyzing possible track changes in the WNP due to climate change, this is the first time that a comprehensive analysis is performed using the same methodology in two large multi-model datasets, as well as synthetic tracks generated from these datasets by statistical-dynamical downscaling.

Our analysis of the TC tracks will be based on two statistical methods. The first is a cluster analysis, which has been extensively applied to observed [*Camargo et al.*, 2007a, b, 2008; *Kossin et al.*, 2010] and model tracks [*Camargo*, 2013; *Daloz et al.*, 2015]. The second is a method previously applied to North Atlantic TC tracks [*Nakamura et al.*, 2009] which synthesizes multiple track characteristics into a few parameters.

By using these two methodologies across two large multi-model datasets, we determine which type of track changes occur most robustly under climate change. Before we examine the climate change question, though, we will use the same methods to determine the capabilities of these models to reproduce the climatological characteristics of observed tracks in the WNP.

The observed and model data are described in section 2. Section 3 covers our methods, sections 4 and 5 present the results for the historical, and future scenarios respectively, and we summarize those results in section 6.

2. Data and Model Simulations

We analyzed WNP TC tracks from two multi-model datasets. The first is that from the U.S. CLIVAR HWG intercomparison. The HWG multi-model dataset consists of a

set of highly idealized experiments using a suite of high-resolution global and regional climate models with the same forcings, most importantly prescribed CO_2 and sea surface temperatures (SSTs) [*Walsh et al.*, 2015], inspired by *Yoshimura and Sugi* [2005] and *Held and Zhao* [2011]. These idealized experiments were chosen in order to gain a better understanding of the response of TC activity to different forcings. Here we consider four different experiments: (i) a control simulation forced with climatological seasonally varying SSTs and sea ice concentrations (1985-2001) and atmospheric gas concentrations from 1992 (called "ctl"); three idealized future simulations, consisting of (ii) a uniform addition of 2K to the control experiment SSTs (plus 2K or "p2K"); (iii) a doubling of the CO_2 concentration (CO2) with the same SSTs; (iv) 2K added to the SSTs and a doubling of CO_2 (p2KCO2). A summary of these simulations is given in Table 1. Many aspects of these simulations have already been examined [*Horn et al.*, 2014; *Patricola et al.*, 2014; *Scoccimarro et al.*, 2014; *Shaevitz et al.*, 2014; *Villarini et al.*, 2014; *Wehner et al.*, 2014; *Camargo et al.*, 2016], but their focus was not in the WNP TC tracks, as considered here. The HWG models included in our analysis are listed in Table 2. The TC tracks were generated by each modeling group, using their standard tracking routines also given in Table 2.

In the case of the MRI model (H8), the simulation designs are not exactly the same as those used in the HWG simulations with the other models, but they are close enough that we decided to incorporate this model in our analysis nonetheless. The MRI simulations are similar to those described in *Sugi et al.* [2012]. For the present climate, the MRI model is forced with monthly observed SST for the period 1979-2003, instead of monthly climatological SST, i.e., the SST varies from year to year, instead of having the same

value in a given calendar month and location in all years. The MRI team defined future SST (FSST) and future CO_2 (FCO2) scenarios based on the average SST and greenhouse gas changes projected by phase 3 of the Coupled Model Intercomparison Project (CMIP3) dataset in the period 2075-2100 for the A1B scenario [*Meehl et al.*, 2007]. The methodology for the construction of FSST and FCO2 is explained in *Sugi et al.* [2012]; *Murakami and Wang* [2010]; *Murakami et al.* [2011]. Three future simulations were performed with the MRI using different SST and CO_2 forcings as follows: (i) future SST (FSST) and current climate CO_2, (ii) present climate SST and future climate CO_2 (FCO2), (iii) 1.83K added uniformly to the present observed SST and future CO2 (p2KFCO2). These simulations were constructed to examine the effect of greenhouse gases and CO_2 separately, as done in the other simulations of the HWG multi-model ensemble.

We also considered fourteen CMIP5 models and simulations. These include the historical runs and one future scenario, RCP8.5, in which greenhouse gas concentrations reach relatively high values in the later years of the 21st century. Only one ensemble member was analyzed for each CMIP5 model and scenario. The models and TCs considered here are the same as those included in *Camargo* [2013] and *Tang and Camargo* [2014]. The TCs were tracked using the Camargo-Zebiak tracking algorithm [*Camargo and Zebiak*, 2002]. The WNP TCs in a subset of these models have already been discussed in *Kossin et al.* [2016]. The list of the CMIP5 models included in our analysis is given in Table 3. The horizontal resolutions in the CMIP5 models are overall much lower than those in the HWG models. It is well known that low-resolution global climate models are able to generate TC-like structures with many similarities to those of observed TCs [*Manabe et al.*, 1970; *Bengtsson et al.*, 1982; *Camargo et al.*, 2005; *Camargo and Wing*, 2016].

However, these TC-like structures are weaker and larger than observed storms, or from high-resolution climate models such as the HWG multi-model dataset. By including the CMIP5 models, however, we are able to span a broader range of future scenarios and models in our analysis, and we judged this sufficient motivation to do so.

The tracking routines used in the HWG and CMIP5 are very similar. They look for features in the model output with a minimum sea-level pressure, maximum low-level vorticity and wind speed and a warm-core. All CMIP5 models used the same tracking algorithm, but with thresholds dependent on model resolution [*Camargo*, 2013]. In contrast, each modeling group applied their own tracking scheme to the HWG models [*Shaevitz et al.*, 2014]. In the case of the HWG models *Horn et al.* [2014] showed that the differences in TC frequency due to tracking algorithm decrease as model resolution increases and TC intensity increases. We examined some specific cases for HWG model tracks, similarly to what was done in *Daloz et al.* [2015] and we could not find any dependence of our results to the tracking routine considered.

In addition to the TC tracks from the explicit simulations from the HWG and the CMIP5 models, we also analyzed tracks produced by statistical-dynamical downscaling from a subset of these models. The downscaling uses the method developed by Emanuel [*Emanuel et al.*, 2006; *Emanuel*, 2006]. The main benefit of this downscaling technique is that it can generate a very large number of synthetic TC tracks with realistic intensities based on environmental fields from reanalyses and climate models. This technique has been successfully applied to generate TC tracks from both reanalysis [*Emanuel*, 2010] and climate models [*Emanuel et al.*, 2008], and has been coupled with storm surge models [*Lin et al.*, 2012].

The Emanuel's downscaling technique is described in detail in *Emanuel* [2006] and *Emanuel et al.* [2006]; here we only give a brief summary. First, synthetic track origin points are generated by seeding randomly the smoothed space-time observed probability distribution function of tropical cyclone genesis. The survival of these seeds depends on its environment. Once the storm is generated, it moves according to the environmental winds vertically averaged over a deep layer of the troposphere, with a correction for the "beta drift" [*Holland*, 1983], similarly to the well known "beta and advection mode"l [*Marks*, 1992]. Once the track is generated, the Coupled Hurricane Intensity Prediction System (CHIPS, *Emanuel et al.* [2004]) is run along each track and determines the storm intensity, as well as when the storm dissipates. The environmental fields necessary to generate the synthetic tracks used here are from the CMIP5 and HWG model simulations.

The CMIP5 synthetic tracks analyzed here have been previously discussed in *Emanuel* [2013]; *Dwyer et al.* [2015]; *Kossin et al.* [2016] and were generated from a subset of the CMIP5 models above. Similarly, synthetic TC tracks were generated from a subset of the HWG models, as discussed in *Daloz et al.* [2015] for the case of the North Atlantic. The list of downscaled models is given in Table 4. Tables 5 and 6 show the numbers of TC tracks in each model and scenario analyzed here.

There are two important caveats in our analysis that should be clearly stated. The first is that when comparing the CMIP5 and HWG explicit tracks, the differences between the HWG and CMIP5 simulations are convolved with the differences in model resolution, which affects TC simulation. The second is that, while the CMIP5 simulations are coupled, the HWG are forced with fixed SSTs, therefore the HWG experiments cannot enforce surface energy balance, which could have potential consequences when simulating TCs,

similarly to the issues due to SST bias in the coupled simulations. Therefore, there is no reason to expect that the track changes in the HWG experiments should be consistent with those in the CMIP5 simulations.

We compared the model TC data with WNP observed TC tracks from the Joint Typhoon Warning Center best-track dataset for the period 1950-2013 [*Chu et al.*, 2002; *JTWC*, 2017].

3. Methods

3.1. Cluster Analysis

We use a cluster analysis method that has been extensively used to analyze TC tracks, both in observations [*Camargo et al.*, 2007a, b, 2008; *Kossin et al.*, 2010; *Ramsay et al.*, 2012] and models [*Camargo*, 2013; *Daloz et al.*, 2015]. This method is described in detail in *Gaffney* [2004] and was first applied to extra-tropical cyclone tracks [*Gaffney et al.*, 2007]. The cluster technique is based on a mixture of polynomial regression models (quadratic here), which are used to fit the shape of the TC tracks. The log likelihood is a goodness of fit metric for probabilistic models. Here the best fit is obtained by maximizing the likelihood that these polynomials fit the data, in this case the longitude and latitude of the tracks. Each model is described by a set of parameters, including regression coefficients and a noise matrix.

The strength of the cluster analysis technique is that it easily fits tracks of different lengths. As is typical in cluster analysis, however, the number of clusters is not uniquely determined, but must be specified a priori. Here we use the same number of clusters that was chosen for observed WNP typhoon tracks, i.e. seven [*Camargo et al.*, 2007a, b]. By

choosing the same number of clusters in models and observations, we can make a direct comparison.

Each model track is assigned to a specific cluster. In the case of the explicit model tracks, there are cases in which there are not many storms per model and scenario (a typical bias of low-resolution models). Therefore, in order to increase the data sample size used in the cluster analysis in each case, we considered the tracks of all scenarios simultaneously for each model as an input of the cluster algorithm. Once each track is assigned to a specific cluster, we can identify to which scenario it belongs.

3.2. Track Moments

A method to distill track shape and length down to a few physically relevant parameters was developed by *Nakamura et al.* [2009]. The entire track shape and length are taken into account to define mass moments of the open curve that defines a storm track. These moments can be used to summarize the statistical characteristics of the storm tracks. The centroid is the first mass moment defining the longitude (X) and latitude (Y) of the center of mass of an individual track or collection of tracks. In the case of an individual track, this centroid lies in the interior of the curve, but not on the curve itself. This first moment determines the location of the effective center of gravity of the individual track or group of tracks. The second mass moments are a measure of the shape of the track or tracks considered. They are defined by the the variance, or the average squared differences of the weighted distances from the centroid and can be expressed geometrically as a covariance ellipse. The variance is then represented by the orientation and length of the principal axes of the ellipse and is a measure of the extent of the tracks in three directions X, Y and XY. By analyzing the location of the centroids and the shape of the ellipses, one is

able to synthesize a large amount of information about the tracks in a very simplified manner. For instance, a rounded variance ellipse implies that the variance in directions X and Y are very similar, while the tilt of the ellipse points to the dominant direction of the track. This method was applied to the North Atlantic hurricane tracks in *Nakamura et al.* [2009], where it is described in detail.

Here we use the ellipses for two purposes: first to compare the model tracks to the observed ones; second to determine the existence of shifts in model tracks under climate change scenarios. The strength of this method is that it uses a simple feature to represent the characteristics of the tracks, either for the whole basin or in each cluster, which makes the comparison with observations and analysis of tracks' shifts simpler than using many tracks or track density.

3.3. Statistical Significance of Track Changes

We tested various characteristics of the tracks to determine if their differences are statistically significant in present and future climates. In order to do that, first a kernel smoothing function estimator (KE) was applied to the distributions of variables in the analysis. KE can increase the signal to noise ratio by making visible the signal that matches the size and shape of the KE. We used the Matlab2012 default KE which employs a normal kernel with an optimized bandwidth. Use of the KE before testing ensures that the continuous distribution of a variable is tested rather than a difference in sampling. Future distributions are estimated at the same points along the axis of the 20C distributions. The future distributions are then re-normalized by multiplying by the ratio of the future KE by the 20C KE.

The Kolmogorov-Smirnov (KS) test is then applied to the control and future scenarios to determine if they are from the same underlying probability distributions at the 0.1-level. The KS test is non-parametric and compares the location and shape of the empirical cumulative distribution functions of the two samples. Once statistical significant changes in the full PDF are identified, the type of the change (e.g. westward/eastward, or larger/smaller) across the multi-model ensembles is examined based on the distribution mean. In order for a track change to be considered statistically significant and robust at least half of the models in each of the multi-model datasets are required to have the same type of statistically significant shift.

4. Present Climate Tracks

4.1. Observations

In *Camargo et al.* [2007a, b] cluster analysis was applied to the observed WNP TC tracks for the period 1950-2005. Here we summarize an updated version of their analysis for the period 1950-2013. The tracks (in grey), genesis positions (red circles) and track ellipses (in black) for all clusters (panels (a) to (g)) and all TCs (panel (h)) are shown in Fig. 8.

The clusters were originally labeled in order of occurrence [*Camargo et al.*, 2007a, b], from the most populated cluster A (361 TCs) to the least populated cluster G (117 TCs). Clusters D and E had a very similar number of storms in the original analysis, 178 and 175 TCs, respectively. In the updated version, cluster D (207 TCs) has slightly fewer TCs than cluster E (216 TCs). Clusters A, C, and E are dominated by recurving TCs, while clusters B, D, and F TCs are mostly straight moving, and G has a combination of both. These clusters depend strongly on the storms' genesis positions. Some track types

are modulated by the El Niño-Southern Oscillation (ENSO): Cluster E TC tracks occur more often in eastern Pacific El Niño events, Cluster G in central Pacific or Modoki El Niño seasons, and Cluster A in La Niña events [*Camargo et al.*, 2007b]. Furthermore, TC tracks in clusters A, B, and E occur more often when the Madden-Julian Oscillation is active over the western North Pacific basin.

The slopes and sizes of the variance ellipses, as well as their centroid locations, emphasize the characteristics of the different clusters in Fig. 8. Straight-moving clusters D and F have very elongated ellipses, while recurving clusters ellipses are more rounded. The slopes of the ellipses differ among the recurving clusters as well. The ellipse of cluster C has a centroid North of 20°N and a northeastward slope, while the ellipses of cluster E and G have centroids south of 20°N and tilt in the northwestward direction.

4.2. Present Climate

The first question we want to examine is whether the models are able to reproduce the observed tracks in the current climate. Given the high number of models, it is impossible to show the tracks of all models and scenarios here, so only the tracks of a few chosen models are shown in Fig. 1. On the left are tracks from the explicit models, while on the right are the tracks of the corresponding downscaled models. Panels (a) and (c) show HWG model tracks, with CMIP5 model tracks in panels (e) and (g) for the control and historical simulations respectively. The centroid of the observed tracks is located near 138°E and 20°N and the models of each type reproduce this well. The explicit models match the slight Southeast to Northwest tilt of the observed tracks, while the downscaled tracks have a distinct Southwest to Northeast tilt. In the tracks this tilt is reflected as a predominately eastward vs. westward movement. For instance, model dH2 in (d) has

more downscaled tracks above 30°N than the corresponding explicit tracks (H2) in (c), enhancing the Southwest to Northeast tilt of the recurving tracks. The explicit model ellipses are smaller both because of the shorter lifetime of tracks as in the case of model H2, as well as the much smaller sample size of the data. There are many more tracks of the downscaled models (see Tables 5 and 6), allowing a wider variance, as the ellipses' variance increases with frequency. Ideally, we would have similar sample sizes, however given the huge computational resources necessary to generate more explicit tracks, this is not possible, and we consider in our analysis all tracks available from all cases. Furthermore, the differences between the explicit and downscaled ellipses could include a contribution from their different termination criteria, as the downscaled tracks allow for extra-tropical transition taking the storms to higher latitudes than the explicit tracks.

We compare the mass moments ellipses of all the models' tracks (shown in Fig. 2) with the observations (Fig. 8(h)). The explicit HWG models have higher horizontal resolution and are more closely grouped than are the CMIP5 explicit models. Some of the CMIP5 explicit models have mass moments that are significantly differently shaped than those in observations, indicating tracks that are not realistic, as was seen for the Atlantic and eastern North Pacific in *Camargo* [2013]. This indicates, in general, that the higher horizontal resolutions of the HWG models lead to more realistic tracks, or could be a result of the inexistence of SST biases, as the HWG simulations are forced with fixed climatological SSTs. It is interesting to notice, though, that the downscaled HWG and CMIP5 models have ellipses with very consistent sizes and shapes. The Southwest to Northeast tilt in the downscaled tracks ellipses occurs in all but one of the models (dH1).

Some of the models have an unrealistically low number of tracks in the present and/or future climates. We need a reasonable sample size in order for the cluster analysis to yield statistically significant results. Similarly to what was done in *Camargo* [2013] and *Kossin et al.* [2016], we exclude the models with very few tracks from the analysis.The models that fall in this category are: MIROC-ESM (M10, total of 43 tracks), NorESM1 (M14, total of 51 tracks), and CAM5.1 LR (H1L, total of 115 tracks) (see Table 6).

We performed a few sensitivity tests on subsets of the model tracks as well. The first test was to examine the role of horizontal resolution in the WNP tracks of the HadGEM3 model, which were available in three different resolutions: H6L, H6M and H6 (see Table 2). There were no significant differences in the mass moments ellipses among these different versions (not shown). Therefore, for the rest of our analysis we considered only the version with the highest horizontal resolution (H6). Even the lowest resolution version of this model has a higher resolution, though, than all the CMIP5 models. This seems to indicate that models with resolutions as low as the CMIP5 models tend to have unrealistic tracks, as indicated by the comparison of panel (c) and panels (a), (b) and (d) in Fig. 2. Once the model resolution is above a certain threshold (in this case 1 deg.), using even higher resolutions will not lead to further improvements in the track characteristics. This issue should be further investigated using more models with multiple horizontal resolutions.

We also compared the tracks obtained by different tracking routines for the model CMCC/ECHAM5 (H2T and H2; not shown). Although the number of tracks generated in each case is different, the overall characteristics of the tracks do not depend on the tracking routine, similar to the result obtained in *Daloz et al.* [2015] for the North Atlantic tracks. Therefore, in the rest of our analysis we will only consider model H2.

We applied the cluster analysis to the remaining models, i.e. excluding M10, M14, H1L, H2T, H6L, H6M. A test to judge model fitness is the similarity of the model tracks to the seven observed clusters. For a model to be considered well-suited for this analysis, identification of at least four of the seven observed clusters was required. In order to do that, we compared the ellipses of the models' and observed clusters. Primarily, the maximum overlapping area of the observed and model ellipses was used to determine to which observed cluster the model cluster corresponded. Secondly, geographic location and ellipse tilt were taken into consideration. Of the twelve explicit CMIP5 models considered here, only six models passed these criteria, namely models M1, M2, M3, M7, M10, and M11. In constrast, all HWG models examined and all of the downscaled CMIP5 and HWG models passed this test. These results corroborate our previous conclusion that high-resolution models generate more realistic model tracks.

The resulting clusters can be seen in Figures 3, 4, 5 for tracks from one model of each type, i.e., explicit CMIP5, explicit HWG and downscaled (from CMIP5). As could be expected from our discussion above, the CMIP5 clusters have some track types that do not occur in reality, e.g. clusters B, D and G (Fig. 3). Both the HWG (Fig. 4) and the CMIP5 downscaled (Fig. 5) clusters tracks are more realistic and more similar to observations, even though some clear biases and differences with observed clusters can still be noted. For instance, both models have problems reproducing the South China Sea storms (straight moving tracks in observed clusters B and D) (Fig. 8). In any case, the large improvement that can be achieved in model tracks by using either higher horizontal resolution or downscaling techniques is very clear in these figures.

5. Future Climate

5.1. Cluster occurrence

The next question we examine is whether there are statistically significant changes in the tracks in the future climate scenarios compared to the historical climate. In addition to assessing statistical significance, we want to determine which changes are robust across many models. We first consider changes in the occurrence of a cluster in the future. Do specific track types become more or less common in the future, and if so, are these changes robust across models?

No statistically significant changes in frequency in the future scenarios were found for the HWG explicit model tracks using the rank sum test at the 0.1 level for all clusters. The rank sum test was chosen as it can be used for testing significance of small populations of unknown distributions. We repeated the same statistical test with the CMIP5 explicit model tracks and the HWG and CMIP5 downscaled tracks. None of these models showed a statistically significant change in the cluster assignment occurrence in future climates, as shown in Fig. 6. We also examined whether the total number of storms in the WNP in each model was statistically different in the future and present climates and again, no model passed the rank sum significance test, even though there is an increase in the number of tracks in the downscaled CMIP5 models as was shown in *Emanuel* [2013].

5.2. Track changes

Next we examine possible changes in the characteristics of the tracks in the future. These changes could be related to shifts in the tracks, or tracks' shape or length. In order to test those possibilities we applied a Kolmogorov-Smirnov (KS) test in present and future climate distributions for each characteristic of the tracks (e.g., longitude of the

ellipse centroid), to determine if they belong to different probabilistic distributions. For a change on a specific direction, e.g. northward or eastward, to be considered statistically significant for a specific cluster or the whole basin, it needs to pass the KS test at the 0.1 level for at least half of the models available for that type of model (HWG or CMIP5) for that cluster, or six or more models for the whole basin. The number six was chosen as it corresponds to half of the number of CMIP5 models (explicit and downscaled) and HWG models (explicit and downscaled) considered in our analysis. However, as discussed above, we could not identify all clusters in all models, therefore, the number of models necessary for significance test in specific clusters, needs to take that into account.

As an example, we show in Fig. 7 the ellipse centroid X kernel distributions for cluster E in the CO2 and control simulations in selected HWG models, as well as cluster F in the RCP85 and historical simulations in selected CMIP5 and downscaled CMIP5 models. Eastward and westward shifts in the means of the distributions can be clearly seen. Some distributions show shifts of the peak westward (model H1), while in others shifts occur in the tails of the distribution (model H7), and in still others shifts are found in both peak and tails (model H6). A similar analysis was performed for all models, clusters and scenarios for various characteristics of the distributions, namely the locations of the centroid ellipses (centroids X and Y), the variances of the ellipses (variance X, Y and XY), their seasonalities, and track lengths.

The variance in the direction X is a measure of the West to East extent of the tracks. The variance in direction Y is a measure of the South to North extent, and the variance in the direction XY is a measure of the tilt, described as a Southwest to Northeast or positive tilt and as Southeast to Northwest or negative tilt extent. These three directional

variances have by far the most number of significant changes in the future distributions when compared with the control or historical simulations. As an example of our analysis, Figure 8 shows that there are changes in cluster A, with significant changes in the variances of Y.

When all tracks in the basin are considered together, there is a net northward movement, in particular in the RCP85 scenario, and a net eastward movement of the straight moving tracks. However, only in one scenario the changes in ellipse characteristics are statistically significant, namely all tracks in p2K scenario (variance X and variance Y), with no statistically significant change for the other scenarios. This could potentially be because changes in one track type cancels changes in other track types. Therefore, in order to examine this possibility, we need to consider track changes in specific clusters.

Given the very large number of models, clusters and scenarios analyzed, only the statistically significant and robust results from our analysis will be discussed here. The most dominant recurving track type (cluster A) has an increase in the variance of Y, which is statistically significant in two HWG scenarios (p2K and CO2) and in the RCP85 CMIP5 scenario. This is consistent with the northward movement noticed for all the tracks in the basin noted above, given that TCs do not form very close to the Equator. Table 7 shows the models and scenarios that have a significant increase in variance of Y for the recurving clusters A, C, E and G. In contrast, the straight moving cluster D has a smaller variance in Y in the HWG scenarios, as well as the straight moving cluster F in the RCP85 scenario. Overall, significant changes in the N-S direction of the tracks were the most frequent in our analysis, though not always consistent across the the HWG and CMIP5 datasets.

Another interesting result is that the tracks in cluster F, which are westward straight moving and can originate in the central Pacific, have an eastward shift in centroid X for the CMIP5 RCP85 scenario (5 out of 11 models), as well a shorter lifespan (5 out of 11 models), as shown in Table 8. Furthermore, some of the HWG models have a decrease of variance in X (6 out of 11 models) and a decrease in the lifespan (6 out of 11 models). As cluster F tracks are straight moving from west to east, both these changes would also result in a net eastward displacement of these tracks. Taking all three changes (centroid X, variance in X and lifetime) into account, the eastward shift in cluster F is clear, though not statistically significant when only considering centroid X changes. As cluster F has genesis locations very close to the date line, this eastward shift would lead to a higher occurrence of central Pacific storms in the future, as previously discussed in the literature [*Li et al.*, 2010; *Murakami et al.*, 2011, 2012; *Yokoi et al.*, 2013; *Mori et al.*, 2013; *Colbert et al.*, 2015; *Roberts et al.*, 2015; *Zhang et al.*, 2017]. This track type is also modulated by the central Pacific or Modoki ENSO. In recent years, there have been very active central Pacific seasons (e.g., Sobel et al. 2016), perhaps with a contribution from anthropogenic climate change [*Murakami et al.*, 2015, 2017]. Cluster G, which can also affect Hawaii, is also the only cluster which has consistent and statistically significant changes for X and Y variances for HWG and CMIP5 scenarios.

In the WNP the variance of XY plays a large role in landfall potential. The main landmass in the basin is located to the West and Northwest. The recurving track shapes of A, C, E, and G tilt toward land when moving from Southeast to Northwest (negative tilt) and away from land when moving Southwest to Northeast (positive tilt). In two of the HWG scenarios (p2K and p2KCO2), there is an eastward shift in cluster A, the most

dominant track type. In contrast, in the CMIP5 models, there is a larger tilt (variance XY) in the RCP85 scenario in three of the clusters (A B and F), with the corresponding tracks, therefore, having a tendency for moving away from land. While the types of shifts are different in both multi-model groups, they lead to a similar consequence.

The location of lifetime maximum intensity (LMI) is another metric of interest. *Kossin et al.* [2014] showed that in observations this metric is less sensitive to non-meteorological data issues. In observations there is a poleward shift in the LMI in some regions, in particular the WNP [*Kossin et al.*, 2014, 2016] and this poleward shift in the WNP is projected to continue in the future under anthropogenic climate change [*Kossin et al.*, 2016].

In the case of the dominant cluster A in CMIP5 there were five models with a statistically significant LMI eastward shift. This eastward shift in the CMIP5 models' cluster A is coherent with the ellipses' eastward shift discussed above. Furthermore, in our analysis overall (including significant and non-significant cases) there were 24 cases (cluster and scenario) of a LMI northward shift out of 47 possible cases, including all of the CMIP5 cases. However, in spite of being a clear dominant shift in the northward direction, very few were statistically significant, including when all tracks in the basin are considered. This northward LMI shift is in qualitative agreement with *Kossin et al.* [2016]. It should be noted tough that the chosen subset of CMIP5 models in *Kossin et al.* [2016] is different from the one here, as different criteria were applied. Secondly, here we used a kernel smoother prior to constructing a probability distribution function and KS statistical test, while in *Kossin et al.* [2016] the probability distribution functions of the latitude of LMI were constructed with the raw model output.

5.3. Environmental field changes

In the previous section we found two primary robust track changes: a poleward shift and an increase in Central Pacific tracks. Both of these changes are coherent with large-scale environmental changes in the models.

There is large body of literature discussing projections of a poleward shift in multiple aspects of the climate system under global warming, mainly in extratropical clouds and storm tracks (e.g., *Yin* [2005]; *Chen and Held* [2007]; *Barnes and Polvani* [2013]; *Tselioudis et al.* [2016]), associated with the weakening and poleward expansion of the Hadley cell under global warming [*Lu et al.*, 2007; *Vecchi and Soden*, 2007]. *Kossin et al.* [2014] showed that the observed LMI poleward shift could be related to changes in the large-scale environment over the past 30 years. *Kossin et al.* [2014] found that changes in vertical wind shear and potential intensity — the latter being the theoretical maximum intensity that a TC can achieve under specified environmental conditions [*Emanuel*, 1988] — have resulted in an expansion in the regions most favorable for TC development. Similarly, in the CMIP5 multi-model mean there is an increase in potential intensity in the whole northern hemisphere, a decrease in the vertical wind shear in the northern part of the basin and an increase in the genesis potential index [*Emanuel and Nolan*, 2004; *Camargo et al.*, 2007c] in the northern part of the basin (see Figs. 12, 13 and 14 in *Camargo* [2013]), which leads to a poleward expansion of the region favorable for TC genesis and intensification. This favorable region also expands into the central North Pacific, making that region more prone to the occurrence of TCs.

Similar analysis of the HWG multi-model ensemble environmental fields is currently in progress and will be the topic of a future publication. Results from the GISS model show

that there is an increase in the potential intensity in the western and central North Pacific for the p2K and p2KCO2 scenarios, accompanied by a decrease of the vertical wind shear and an increase in the tropical cyclone genesis index [*Tippett et al.*, 2011; *Camargo et al.*, 2014] in the eastern part of the basin, leading to an expansion of the area that is favorable for TC occurrence poleward and eastward (Figs. 10, 11, and 13 in *Camargo et al.* [2016]).

Another metric of the environment's favorability for TC occurrence and intensification is the ventilation index, which combines vertical wind shear (between 850 and 250hPa), potential intensity and entropy deficit (defined using the ratio of the differences of the saturated and moist entropy value at 700hPa, and the sea surface and boundary layer) [*Tang and Emanuel*, 2012].

In the CMIP5 models there is a general tendency towards an increase in the seasonal ventilation index with warming in most basins, including the deep tropical region of the western North Pacific, which would inhibit both tropical cyclogenesis and intensification [*Tang and Camargo*, 2014]. In the CMIP5 multimodel mean this increase has a maximum around 10°N and 160°W, decreasing poleward and eastward of there. This change pattern would lead to a reduction of TC activity in the southern part of the basin and an increase poleward. There is also a decrease in the ventilation index in the central North Pacific, helping to explain the increase of TC activity near Hawaii. In summary, the large-scale environment in the CMIP5 projections and in the HWG GISS model simulations are coherent with the poleward and eastward track shifts discussed above.

6. Conclusions

We analyzed TC tracks in the Western North Pacific (WNP) basin in two large multi-model ensembles. These ensembles span a variety of model types (low and high horizontal

resolution models, models forced with fixed SST and coupled models) and tracks (explicit and downscaled). We used two primary methodologies to examine the tracks' characteristics: a cluster analysis and mass moment ellipses. We applied these methods first to compare the model tracks with observed tracks, and second to examine if there are changes in the tracks in a warming climate that are statistically significant and robust across the ensembles. The impact of tracking methodologies on our analysis was explored and our results do not depend on the tracking method for the cases analyzed. Furthermore, it should be noted that changes in genesis locations cannot be separated from the track changes by this methodology, as the genesis locations are inherently part of the detected tracks and the thresholds used in the different tracking algorithms.

The HWG models' explicit tracks are much more similar to observed tracks than are the CMIP5 explicit tracks. This indicates that, all else equal, higher horizontal resolution yields more realistic tracks. However, an improvement with resolution was not apparent when comparing the tracks from three versions of an HWG model in three resolutions[2], with no additional modifications in the model. The downscaled tracks have a northeastward bias which is present in both the HWG and CMIP5 downscaled model tracks, indicating that these biases were not dependent on the models' large-scale environments, but rather appear to be features of the downscaling methodology.

We examined many characteristics of WNP tracks to determine if there were statistically significant and robust changes in future scenarios. There is an increase in variance of Y, or South to North extent of the range over which the tracks occur for several models and clusters. As WNP tropical cyclones are bound on the southern end by the vanishing of the Coriolis parameter at the equator, this can be interpreted as a northern shift of the

WNP TC tracks. This northern shift is not statistically significant at a particular point, such as the mean (centroid) or the LMI, but is very robust in the variance or extent of the model tracks.

There were also many models and scenarios that show eastern and northeastern shifts. As the WNP basin is bound on the west side by the Asian landmass, an extension in the variance of X can be interpreted as an eastern movement and an extension in the variance of XY as a northeastward movement. However, in most cases, the shifts in the centroid location are too small to be statistically significant, even when the variance shifts are statistically significant.

Some of the track changes described here have been previously noticed in the literature, to the extent that they are apparent in the statistics of the set of all WNP tracks. Here we pinpoint which track types, as defined by cluster analysis, are involved in specific track shifts. In some clusters, there is an increase in the variance in the latitudinal direction, while in others there is an eastward shift.

For the most frequent track type, recurving cluster A, while the centroid shifts are small, there is an increase in the South-North extent of the tracks with warming in both the HWG and CMIP5 simulations, effectively corresponding to a northward shift in the tracks. This is an important result, as cluster A has impacts throughout the region and occurs more commonly in La Niña events. Shifts in cluster A tracks could lead to significant changes in the landfall occurrences, as discussed in *Kossin et al.* [2016].

Another interesting case is the straight moving Cluster F, which has an eastward mean shift in the centroid for CMIP5 models, which could lead to more storms in the Central Pacific and Hawaii. The other cluster with potential influence in Hawaii is the recurving

cluster G. While there was no significant mean centroid location change for cluster G, the variance in both longitudinal and latitudinal directions increased in two of the HWG scenarios, which could be interpreted as an eastward (towards Hawaii) shift in the storms' preferred formation region accompanied by a poleward shift in recurvature when compared to the 20th century control simulation.

Changes in the large-scale environment in the CMIP5 multi-model mean and in the GISS model in the HWG dataset are coherent with the statistically significant and robust changes in track properties in the WNP. These were, for instance a poleward expansion of the areas with high potential intensity, and increased values of the ventilation index in the CMIP5 models. Our results highlight the complexity of potential track changes in future climates, with different shifts occurring simultaneously for different track types. Furthermore, these track shifts are model- and scenario-dependent, highlighting the value of considering multiple models and scenarios when inferring robust changes in TC tracks in future climates. The upcoming multi-resolution multi-model simulations planned for CMIP6 will be a good opportunity to explore robust the future track changes using high-resolution coupled models [*Haarsma et al.*, 2016].

Acknowledgments. The authors acknowledge the support from the following grants: NASA NNX09AK34G, NNX13AM18G, NSF AGS 1143959, and NOAA NA11OAR4310093. MR was supported by the Joint UK BEIS/Defra Met Office Hadley Centre Climate Programme (GA01101). MFW contribution to this work is supported by the Regional and Global Climate Modeling Program of the Office of Biological and Environmental Research in the Department of Energy Office of Science under contract number DE-AC02-05CH11231. PLV acknowledges support from the PRACE-UPSCALE

project. We would like to thank the members of the U.S. CLIVAR Hurricane Working Group and Naomi Henderson for making the model data available for the Hurricane Working Group and managing the Hurricane Working Group dataset. The track model data can be made available by individual request for research purposes by contacting the corresponding author Suzana Camargo (suzana@ldeo.columbia.edu). The JTWC best-track dataset is available at `https://metoc.ndbc.noaa.gov/web/guest/jtwc/best_tracks/western-pacific`.

Notes

1. Tropical cyclone-like structures are defined by a local minimum in sea-level pressure, a local maximum in low-level relative humidity and a warm core.

2. Even the lowest resolution of this model has a finer resolution than the CMIP5 models

References

Bao, Q., P. Lin, T. Zhou, Y. Liu, Y. Yu, G. Wu, B. He, J. He, L. Li, J. Li, Y. Li, H. Liu, F. Qiao, Z. Song, B. Wang, J. Wang, P. Wang, X. Wang, Z. Wang, B. Wu, T. Wu, Y. Xu, H. Yu, W. Zhao, W. Zheng, and L. Zhou (2013), The Flexible Global Ocean-Atmosphere-Land system model, spectral version 2: FGOALS-s2, *Adv. Atmos. Sci.*, *30*, 561–576, doi:10.1007/s00376-012-2113-9.

Barnes, E. A., and L. M. Polvani (2013), Response of the midlatitude jets, and of their variability, to increased greenhouse gases in the CMIP5 models, *J. Climate*, *26*, 7117–7135, doi:10.1175/JCLI-D-12-00536.1.

Bengtsson, L., H. Böttger, and M. Kanamitsu (1982), Simulation of hurricane-type vortices in a general circulation model, *Tellus*, *34*, 440–457.

Bengtsson, L., K. I. Hodges, and M. Esch (2007a), Tropical cyclones in a T159 resolution global climate model: Comparison with observations and re-analysis, *Tellus*, *59 A*, 396–416.

Bengtsson, L., K. I. Hodges, M. Esch, N. Keenlyside, L. Kornblueh, J.-J. Luo, and T. Yamagata (2007b), How many tropical cyclones change in a warmer climate?, *Tellus*, *59 A*, 539–561.

Camargo, S. J. (2013), Global and regional aspects of tropical cyclone activity in the CMIP5 models, *J. Climate*, *26*, 9880–9902, doi:10.1175/JCLI-D-12-00549.1.

Camargo, S. J., and A. A. Wing (2016), Tropical cyclones in climate models, *WIREs Clim. Change*, *7*, 211–237, doi:10.1002/wcc373.

Camargo, S. J., and S. E. Zebiak (2002), Improving the detection and tracking of tropical storms in atmospheric general circulation models, *Wea. Forecasting*, *17*, 1152–1162.

Camargo, S. J., A. G. Barnston, and S. E. Zebiak (2005), A statistical assessment of tropical cyclones in atmospheric general circulation models, *Tellus*, *57A*, 589–604, doi: 10.1111/j.1600-0870.2005.00117.x.

Camargo, S. J., A. W. Robertson, S. J. Gaffney, P. Smyth, and M. Ghil (2007a), Cluster analysis of typhoon tracks. Part I: General properties, *J. Climate*, *20*, 3635 – 3653.

Camargo, S. J., A. W. Robertson, S. J. Gaffney, P. Smyth, and M. Ghil (2007b), Cluster analysis of typhoon tracks. Part II: Large-scale circulation and ENSO, *J. Climate*, *20*, 3654 – 3676.

Camargo, S. J., K. A. Emanuel, and A. H. Sobel (2007c), Use of a genesis potential index to diagnose ENSO effects on tropical cyclone genesis, *J. Climate*, *20*, 4819–4834.

Camargo, S. J., A. W. Robertson, A. G. Barnston, and M. Ghil (2008), Clustering of eastern North Pacific tropical cyclone tracks: ENSO and MJO effects, *Geochem. Geophys. and Geosys.*, *9*, Q06V05, doi:10.1029/2007GC001861.

Camargo, S. J., M. K. Tippett, A. H. Sobel, G. A. Vecchi, and M. Zhao (2014), Testing the performance of tropical cyclone genesis indices in future climates using the HIRAM model, *J. Climate*, *27*, 9171–9196.

Camargo, S. J., A. H. Sobel, A. D. D. Genio, J. A. Jonas, M. Kelley, Y. Lu, D. A. Shaevitz, and N. Henderson (2016), Tropical cyclones in the GISS ModelE2, *Tellus A*, *68*, 31,494, doi:10.3402/tellusa.v68.31494.

Chen, G., and I. M. Held (2007), Phase speed spectra and the recent poleward shift of southern hemisphere surface westerlies, *Geophys. Res. Lett.*, *34*, L21,805, doi:10.1029/2007GL031200.

Chu, J.-H., C. R. Sampson, A. S. Levine, and E. Fukada (2002), The Joint Typhoon Warning center tropical cyclone best-tracks, 1945-2000, *Tech. Rep. NRL/MR/7540-02-16*, Naval Research Laboratory.

Colbert, A. J., B. J. Soden, and B. P. Kirtman (2015), The impact of natural and anthropogenic climate change on western North Pacific tropical cyclone tracks, *J. Climate*, *28*, 1806–1823.

Daloz, A. S., and S. J. Camargo (2017), Is the poleward migration of tropical cyclone maximum intensity associated with a poleward migration of tropical cyclone genesis?, *Clim. Dyn.*, doi:10.1007/s00382-017-3636-7, early online.

Daloz, A. S., S. J. Camargo, J. P. Kossin, K. Emanuel, M. Horn, J. A. Jonas, D. Kim, T. LaRow, Y.-K. Lim, C. M. Patricola, M. Roberts, E. Scoccimarro, D. Shaevitz, P. L.

Vidale, H. Wang, M. Wehner, and M. Zhao (2015), Cluster analysis of explicitly and downscaled simulated North Atlantic tropical cyclone tracks, *J. Climate*, *28*, 1333–1361, doi:10.1175/JCLI-D-13-00646.1.

Donner, L. J., B. L. Wyman, R. S. Hemler, L. W. Horowitz, Y. Ming, M. Zhao, J.-C. Golaz, P. Ginoux, S.-J. Lin, M. D. Schwarzkopf, J. Austin, G. Alakac, W. F. Cooked, T. L. Delworth, S. M. Freidenreich, C. T. Gordon, S. M. Griffies, I. M. Held, T. R. K. William J. Hurlina, Stephen A. Kleine, A. R. Langenhorst, H.-C. Lee, Y. Lin, B. I. Magi, S. L. Malyshev, P. C. D. Milly, V. Naik, M. J. Nath, R. Pincus, J. J. Ploshay, V. Ramaswamy, C. J. Seman, E. Shevliakova, J. J. Sirutis, W. F. Stern, R. J. Stouffer, R. J. Wilson, M. Winton, A. T. Wittenberg, , and F. Zeng (2011), The dynamical core, physical parameterizations, and basic simulation characteristics of the atmospheric component of the GFDL global coupled model CM3, *J. Climate*, *24*, 34843519, doi: 10.1175/2011JCLI3955.1.

Dwyer, J. G., S. J. Camargo, A. H. Sobel, M. Biasutti, K. A. Emanuel, G. A. Vecchi, M. Zhao, and M. K. Tippett (2015), Projected 21st century changes in the length of the tropical cyclone season, *J. Climate*, *28*, 1333–1361, doi:10.1175/JCLI-D-13-00646.1.

Emanuel, K. (2006), Climate and tropical cyclone activity: A new model downscaling approach, *J. Climate*, *19*, 4797–4802.

Emanuel, K. (2010), Tropical cyclone activity downscaled from NOAA-CIRES reanalysis, 1908-1958, *J. Adv. Model. Earth Syst.*, *2*, 1, doi:10.3894/JAMES.2010.2.1.

Emanuel, K., C. DesAutels, C. Holloway, and R. Korty (2004), Environmental control of tropical cyclone intensity, *J. Atmos. Sci.*, *61*, 843–858.

Emanuel, K., S. Ravela, E. Vivant, and C. Risi (2006), A statistical deterministic approach to hurricane risk assessment, *Bull. Amer. Meteor. Soc.*, *87*, 299–314.

Emanuel, K., R. Sundararajan, and J. Williams (2008), Hurricanes and global warming: Results from downscaling IPCC AR4 simulations, *Bull. Amer. Meteor. Soc.*, *99*, 347–367.

Emanuel, K. A. (1988), The maximum intensity of hurricanes, *J. Atmos. Sci.*, *45*, 1143–1155.

Emanuel, K. A. (2013), Downscaling CMIP5 climate models shows increased tropical cyclone activity over the 21st century, *Proc. Nat. Acad. Sci.*, *110*, 12,219–12,224, doi: 10.1073/pnas.1301293110.

Emanuel, K. A., and D. S. Nolan (2004), Tropical cyclone activity and global climate, *Bull. Amer. Meteor. Soc.*, *85*, 666–667.

Gaffney, S. J. (2004), Probabilistic curve-aligned clustering and prediction with regression mixture models, Ph.D. thesis, Department of Information and Computer Science, University of California, Irvine, CA.

Gaffney, S. J., A. W. Robertson, P. Smyth, S. J. Camargo, and M. Ghil (2007), Probabilistic clustering of extratropical cyclones using regression mixture models, *Clim. Dyn.*, *29*, 423–440, doi:10.1007/s00382-007-0235-z.

Gent, P. R., G. Danabasoglu, L. J. Donner, M. M. Holland, E. C. Hunke, S. R. Jayne, D. M. Lawrence, R. B. Neale, P. J. Rasch, M. Vertenstein, P. H. Worley, Z. L. Yang, and M. Zhang (2011), The Community Climate System Model version 4, *J. Climate*, *24*, 4973–4991, doi:10.1175/2011JCLI4083.1.

Haarsma, R. J., M. Roberts, P. L. Vidale, C. A. Senior, A. Bellucci, Q. Bao, P. Chang, S. Corti, N. S. Fučkar, V. Guemas, J. von Hardenberg, W. Hazeleger, C. Kodama, T. Koenigk, L. R. Leung, J. Lu, J.-J. Luo, J. Mao, M. S. Mizielinski, R. Mizuta, P. Nobre, M. Satoh, E. Scoccimarro, T. Semmler, J. Small, and J.-S. von Storch (2016), High resolution model intercomparison project (HighResMIP), *Geosci. Model Dev. Discuss.*, doi:10.5194/gmd-2016-66.

Hall, T. M., and A. H. Sobel (2013), On the impact angle of Hurricane Sandy's New Jersey landfall, *Geophys. Res. Lett.*, *40*, 2312–2315, doi:10.1002/grl.50395.

Held, I. M., and M. Zhao (2011), The response of tropical cyclone statistics to an increase in CO_2 with fixed sea surface temperatures, *J. Climate*, *20*, 5353–5364.

Hodges, K. I. (1995), Feature tracking on the unite sphere, *Mon. Wea. Rev.*, *19*, 5686–5699.

Holland, G. J. (1983), Tropical cyclone motion: Environmental interaction plus a beta effect, *J. Atmos. Sci.*, *40*, 328–342.

Horn, M., K. Walsh, M. Zhao, S. J. Camargo, E. Scoccimarro, H. Murakami, H. Wang, A. Ballinger, A. Kumar, D. A. Shaevitz, J. A. Jonas, and K. Oouchi (2014), Tracking scheme dependence of simulate tropical cyclone response to idealized climate simulations, *J. Climate*, *27*, 9197–9213.

Jones, C. D., J. K. Hughes, N. Bellouin, S. C. Hardiman, G. S. Jones, J. Knight, S. Liddicoat, F. M. O'Connor, R. J. Andres, C. Bell, K.-O. Boo, A. Bozzo, N. Butchart, P. Cadule, K. D. Corbin, M. Doutriaux-Boucher, P. Friedlingstein, J. Gornall, L. Gray, P. R. Halloran, G. Hurtt, W. J. Ingram, J.-F. Lamarque, R. M. Law, M. Meinshausen, S. Osprey, E. J. Palin, L. P. Chini, T. Raddatz, M. G. Sanderson, A. A. Sellar,

A. Schurer, P. Valdes, N. Wood, S. Woodward, M. Yoshioka, and M. Zerroukat (2011), The HadGEM2-ES implementation of CMIP5 centennial simulations, *Geosci. Model. Dev.*, *4*, 453–470, doi:10.5194/gmd-4-543-2011.

JTWC (2017), Joint Typhoon Warning Center Tropical Cyclone Best Track Data Site, Available online at https://metoc.ndbc.noaa.gov/web/guest/jtwc/best_tracks.

Knutson, T. R., J. McBride, J. Chan, K. A. Emanuel, G. Holland, C. Landsea, I. Held, J. Kossin, A. K. Srivastava, and M. Sugi (2010), Tropical cyclones and climate change, *Nat. Geosci.*, *3*, 157–163, doi:10.1038/ngeo779.

Knutson, T. R., J. J. Sirutis, M. Zhao, R. E. Tuleya, M. Bender, G. A. Vecchi, G. Villarini, and D. Chavas (2015), Global projections of intense tropical cyclone activity for the late twenty-first century from dynamical downscaling of CMIP5/RCP4.5 scenarios, *J. Climate*, *28*, 7203–7224, doi:10.1175/JCLI-D-15-0129.1.

Kossin, J. P., S. J. Camargo, and M. Sitkowski (2010), Climate modulation of North Atlantic hurricane tracks, *J. Climate*, *23*, 3057–3076, doi:10.1175/2010JCLI3497.1.

Kossin, J. P., K. A. Emanuel, and G. A. Vecchi (2014), The poleward migration of the location of tropical cyclone maximum intensity, *Nature*, *509*, 349–352.

Kossin, J. P., K. A. Emanuel, and S. J. Camargo (2016), Past and projected changes in western North Pacific tropical cyclone exposure, *J. Climate*, *29*, 5725–5739, doi:10.1175/JCLI-D-16-0076.1.

Lander, M., C. Guard, and S. J. Camargo (2014), Tropical cyclones, super-typhoon Haiyan, in *State of the Climate in 2013*, *Bull. Amer. Meteor. Soc.*, vol. 95, edited by J. Blunden and D. S. Arndt, pp. S112–S114, American Meteorological Society, doi:10.1175/2014BAMSStateoftheClimate.1.

LaRow, T. E., Y.-K. Lim, D. W. Shin, E. P. Chassignet, and S. Cocke (2008), Atlantic basin seasonal hurricane simulations, *J. Climate*, *21*, 3191–3206.

Li, T., M. Kwon, M. Zhao, J.-S. Kug, J.-J. Luo, and W. Yu (2010), Global warming shifts Pacific tropical cyclone location, *Geophys. Res. Lett.*, *37*, L21, 804, doi:10.1029/2010GL045124.

Liang, A., L. Oey, S. M. Shiming, and S. Chou (2017), Long-term trends of typhoon-induced rainfall over Taiwan: In situ evidence of poleward shift of typhoons in western North Pacific in recent decades, *J. Geophys. Res.*, *122*, 2750–2765, doi:10.1002/2017JD026446.

Lin, I.-I., and J. C. L. Chan (2015), Recent decrease in typhoon destructive potential and global warming implications, *Nature Comm.*, *6*, 7182, doi:10.1038/ncomms8182.

Lin, I.-I., I.-F. Pun, and C.-C. Lien (2014), "Category-6" supertyphoon Haiyan in global warming hiatus: Contribution from sub-surface ocean warming, *Geophys. Res. Lett.*, *41*, 8547–8553, doi:10.1002/2014GL061281.

Lin, N., K. Emanuel, M. Oppenheimer, and E. Vanmarcke (2012), Physically based assessment of hurricane surge threat under climate change, *Nature Clim. Change*, *2*, 462–467.

Lu, J., G. A. Vecchi, and T. Reichler (2007), Expansion of the Hadley cell under global warming, *Geophys. Res. Lett.*, *34*, L06,805, doi:10.1029/2006GL028443.

Manabe, S., J. L. Holloway, and H. M. Stone (1970), Tropical circulation in a time-integration of a global model of the atmosphere, *J. Atmos. Sci.*, *27*, 580–613.

Manganello, J. V., K. I. Hodges, B. Dirtmeyer, J. L. Kinter, B. A. Cash, L. Marx, T. Jung, D. Achuthavarier, J. M. Adams, E. L. Altshuler, B. Huang, E. K. Jin, P. Towers, and N. Wedi (2014), Future changes int he western North Pacific tropical cyclone activ-

ity projected by a multidecadal simulation with a 16-km global atmospheric GCM, *J. Climate*, *27*, 7622–7646.

Marks, D. G. (1992), The beta and advection model for hurricane track forecasting, *NOAA Tech. Memo. NWS NMC 70*, National Meteorological Center, Camp Springs, MD, 89pp.

Meehl, G., C. Covey, T. Delworth, M. Latif, B. McAvaney, J. Mitchell, R. Stouffer, and K. Taylor (2007), The WCRP CMIP3 multimodel dataset: A new era in climate change research, *Bull. Amer. Meteor. Soc.*, *88*, 13831394.

Mei, W., and S.-P. Xie (2016), Intensification of landfalling typhoons over the northwest Pacific since the late 1970s, *Nature Geos.*, *9*, 753–757, doi:10.1038/ngeo2792.

Mizuta, R., H. Yoshimura, H. Murakami, M. Matsueda, H. Endo, T. Ose, K. Kamiguchi, M. Hosaka, M. Sugi, S. Yukimoto, S. Kusunoki, and A. Kitoh (2012), Climate simulations using the improved MRI-AGCM with 20-km grid, *J. Meteor. Soc. Japan*, *90A*, 235–260.

Mori, M., M. Kimoto, M. Ishi, S. Yokoi, T. Mochikuzi, Y. Chikamoto, M. Watanabe, T. Nokazawa, H. Tatebe, T. T. Sakamoto, Y. Komuro, Y. Imada, and H. Koyama (2013), Hindcast prediction and near-future projection of tropical cyclone activity over the western North Pacific using CMIP5 near-term experiments with MIROC, *J. Meteo. Soc. Japan*, *91*, 431–452, doi:10.2151/jmsj.2013-402.

Murakami, H., and B. Wang (2010), Future change of north atlantic tropical cyclone tracks: Projection by a 20-km-mesh global atmospheric model, *J. Climate*, *23*, 2569–2584, doi:10.1175/2010JCLI3338.1.

Murakami, H., B. Wang, and A. Kitoh (2011), Future change of Western North Pacific typhoons: Projections by a 20-km-mesh global atmospheric model, *J. Climate*, *24*,

1154–1169, doi:10.1175/2010JCLI3723.1.

Murakami, H., Y. Wang, H. Yoshimura, R. Mizuta, M. Sugi, E. Shindo, Y. Adachi, S. Yukimoto, M. Hosaka, S. Kusunoki, T. Ose, and A. Kitoh (2012), Future changes in tropical cyclone activity projected by the new high-resolution MRI-AGCM, *J. Climate*, *25*, 3237–3260.

Murakami, H., P.-C. Hsu, O. Arakawa, and T. Li (2014), Influence of model biases on projected future changes in tropical cyclone frequency of occurrence, *J. Climate*, *27*, 2159–2181.

Murakami, H., G. A. Vecchi, T. Delworth, K. Paffendorf, R. Gudgel, L. Jia, and F. Zheng (2015), Investigating the influence of anthropogenic forcing and natural variability on the 2014 Hawaiian hurricane season, in *Bull. Amer. Meteor. Soc.*, *Explaining extremes of 2014 from a climate perspective*, vol. 96, pp. S115–S119, American Meteorological Society.

Murakami, H., G. A. Vecchi, T. L. Delworth, A. T. Wittenberg, S. Underwood, R. Gudgel, X. Yang, L. Jia, F. Zeng, K. Paffendorf, and W. Zhang (2017), Dominant role of subtropical Pacific warming in extreme eastern Pacific hurricane seasons: 2015 and the future, *J. Climate*, *30*, 243–264, doi:10.1175/JCLI-D-16-0424.1.

Nakamura, J., U. Lall, Y. Kushnir, and S. J. Camargo (2009), Classifying North Atlantic tropical cyclones tracks by their mass moments, *J. Climate*, *22*, 5481–5494, doi:10.1175/2009JCLI2828.1.

Patricola, C. M., R. Saravanan, and P. Chang (2014), The impact of the El-Niño-Southern Oscillation and Atlantic Meridional Mode on seasonal tropical cyclone activity, *J. Climate*, *27*, 5311–5328.

Prabhat, O. Rubel, S. Byna, K. S. Wu, M. Wehner, and W. Bethel (2012), TECA: A parallel toolkit for extreme climate analysis, in *Proc. Int. Conf. on Computational Science, ICCS 2012*, *Procedia Computer Science*, vol. 9, edited by H. Ali, Y. Shi, D. Khazanchi, M. Lees, G. VanAlbada, J. Dongarra, and P. M. A. Sloot, pp. 866–876.

Ramsay, H. A., S. J. Camargo, and D. Kim (2012), Cluster analysis of tropical cyclone tracks in the southern hemisphere, *Clim. Dyn.*, *39*, 897–917.

Roberts, M. J., P. L. Vidale, M. S. Mizienlinski, M.-E. Demory, R. Schiemann, J. Strachan, K. Hodges, R. Bell, and J. Camp (2015), Tropical cyclones in the UPSCALE ensemble of high-resolution global climate models, *J. Climate*, *28*, 574–596, doi: 10.1175/JCLI-D-14-00131.1.

Roeckner, E., G. Bäuml, L. Bonaventura, R. Brokopf, M. Esch, M. Giorgetta, S. Hagemann, L. Kornblueh, U. Schlese, U. Schulzweida, I. Kirchner, E. Manzini, A. Rhodin, and A. Tompkins (2003), The atmospheric general circulation model ECHAM5. Part I: Model description, *Tech. Rep. 349*, Max-Planck Institute for Meteorology, Hamburg, Germany, 127 pp.

Rotstayn, L. D., S. J. Jeffrey, M. A. Collier, S. M. Dravitzki, A. C. Hirst, J. I. Syktus, and K. K. Wong (2012), Aerosol- and greenhouse gas-induced changes in summer rainfall and circulation in the Australasian region: a study using single-forcing climate simulations, *Atmos. Chem. Phys.*, *12*, 6377–6404, doi:10.5194/acp-12-6377-2012.

Saha, S., S. Moorthi, X. Wu, J. Wang, S. Nadiga, P. Tripp, D. Behringer, Y.-T. Hou, H.-Y. Chuang, M. Iredell, M. Ek, J. Meng, R. Yang, M. P. Mendez, H. van den Dool, Q. Zhang, W. Wang, M. Chen, and E. Becker (2014), The NCEP climate forecast system version 2, *J. Climate*, *27*, 2185–2208.

Schmidt, G. A., M. Kelley, L. Nazarenko, R. Ruedy, G. L. Russell, I. Aleinov, M. Bauer, S. E. Bauer, M. K. Bhat, R. Bleck, V. Canuto, Y. H. Chen, Y. Cheng, T. L. Clune, A. Del Genio, R. de Fainchtein, G. Falugevi, J. E. Hansen, R. J. Healy, N. Y. Kiang, D. Koch, A. A. Lacis, A. N. LeGrande, J. Lerner, K. K. Lo, E. E. Matthews, S. Menon, R. L. Miller, V. Oinas, A. O. Oloso, J. P. Perlwitz, M. J. Puma, W. M. Putman, D. Rind, A. Romanou, M. Sato, D. T. Schindell, S. Sun, R. A. Syed, N. Tausnev, K. Tsigaridis, N. Unger, A. Voulgarakis, M.-S. Yao, and J. Zhang (2014), Configuration and assessment of GISS ModelE2 contributions to the CMIP5 archive, *J. Adv. Model. Earth Syst.*, *6*, 141–184.

Scoccimarro, E., S. Gualdi, A. Bellucci, A. Sanna, P. G. Fogli, E. Manzini, M. Vichi, P. Oddo, and A. Navarra (2011), Effects of tropical cyclones on ocean heat transport in a high resolution coupled general circulation model, *J. Climate*, *24*, 4368–4384.

Scoccimarro, E., S. Gualdi, G. Villarini, G. A. Vecchi, M. Zhao, K. Walsh, and A. Navarra (2014), Increased precipitation events associated with landfalling tropical cyclones in response to a warmer climate and increased CO_2, *J. Climate*, *27*, 4642–4654, doi:10.1175/JCLI-D-14-00065-1.

Shaevitz, D. A., S. J. Camargo, A. H. Sobel, J. A. Jonas, D. Kim, A. Kumar, T. LaRow, Y.-K. Lim, H. Murakami, K. A. Reed, M. J. Roberts, E. Scoccimarro, P. L. Vidale, H. Wang, M. F. Wehner, M. Zhao, and N. Henderson (2014), Characteristics of tropical cyclones in high-resolution models of the present climate, *J. Adv. Model Earth Syst.*, *6*, 1154–1172, doi:10.1002/2014MS000372.

Sobel, A. H., S. J. Camargo, A. G. Barnston, and M. K. Tippett (2016), Northern hemisphere tropical cyclones during the quasi-El Niño of late 2014, *Nat. Haz.*, *83*, 1717–1729,

doi:10.1007/s11069-016-2389-7.

Sugi, M., H. Murakami, and J. Yushimura (2012), On the mechanism of tropical cyclone frequency changes due to global warming, *J. Meteor. Soc. Japan*, *90A*, 397–408, doi: 10.2151/jmsj.2012-A24.

Tang, B., and S. J. Camargo (2014), Environmental control of tropical cyclones in CMIP5: A ventilation perspective, *J. Adv. Model. Earth Syst.*, *6*, 115–128, doi: 10.1002/2013MS000294.

Tang, B., and K. Emanuel (2012), A ventilation index for tropical cyclones, *Bull. Amer. Meteor. Soc.*, *93*, 1901–1912, doi:10.1175/BAMS-D-11-00165.2.

Taylor, K. E., R. J. Stouffer, and G. A. Meehl (2012), An overview of CMIP5 and the experiment design, *Bull. Amer. Meteor. Soc.*, *93*, 485–498.

Tippett, M. K., S. J. Camargo, and A. H. Sobel (2011), A Poisson regression index for tropical cyclone genesis and the role of large-scale vorticity in genesis, *J. Climate*, *24*, 2335–2357, doi:10.1175/2010JCLI3811.1.

Tory, K. J., S. S. Chand, J. L. McBride, H. Ye, and R. A. Dare (2013), Projected changes in late-twenty-first-century tropical cyclone frequency in 13 coupled climate models from phase 5 of the Coupled Model Intercomparison Project, *J. Climate*, *26*, 9946–9959, doi:10.1175/JCLI-D-32-00010.1.

Tselioudis, G., B. R. Lipat, D. Konsta, K. M. Grise, and L. M. Polvani (2016), Midlatitude cloud shifts, their primary link to the Hadley cell, and their diverse radiative effects, *Geophys. Res. Lett.*, *43*, 4594–4601, doi:10.1002/2016GL068242.

Vecchi, G. A., and B. J. Soden (2007), Global warming and the weakening of the tropical circulation, *J. Climate*, *20*, 4316–4340, doi:10.1175/JCLI4258.1.

Villarini, G., and G. A. Vecchi (2012), Twenty-first-century projections of north atlantic tropical storms from CMIP5 models, *Nature Clim. Change*, *2*, 604–607.

Villarini, G., D. A. Lavers, E. Scoccimarro, M. Zhao, M. F. Wehner, G. A. Vecchi, T. R. Knutson, and K. A. Reed (2014), Sensitivity of tropical cyclone rainfall to idealized global scale forcings, *J. Climate*, *27*, 4622–4641, doi:10.1175/JCLI-D-13-00780.1.

Vitart, F., D. Anderson, and T. Stockdale (2003), Seasonal forecasting of tropical cyclone landfall over Mozambique, *J. Climate*, *16*, 3932–3945.

Voldoire, A., E. Sanchez-Gomez, D. S. y Mélia, B. Decharme, C. Cassou, S. Sénési, S. Valcke, I. Beau, A. Alias, M. Chevallier, M. Déqué, J. Deshayes, H. Douville, E. Fernandez, G. Madec, E. Maisonnave, M.-P. Moine, S. Planton, D. Saint-Martin, S. Szopa, S. Tyteca, R. Alkama, S. Belamari, A. Braun, L. Coquart, and F. Chauvin (2013), The CNRM-CM5.1 global climate model: description and basic evaluation, *Clim. Dyn.*, *40*, 2091–2121, doi:10.1007/s00382-011-1259-y.

Volodin, E. M., N. A. Dianskii, and A. V. Gusev (2010), Simulating present-day climate with INMCM4.0 coupled model of the atmospheric and oceanic general circulations, *Atm. Ocean Phys.*, *46*, 414–431, doi:10.1134/S000143381004002X.

von Salzen, K., J. F. Scinocca, N. A. Farlane, J. N. Lie, J. N. S. Cole, D. Plummer, D. Verseghy, M. C. Reader, X. Y. Ma, M. Lazare, and L. Solheim (2013), The Canadian fourth generation atmospheric global climate model (CanAM4). Part I: Representation of physical processes, *Atmosphere-Ocean*, *51*, 104–125, doi:10.1080/07055900.2012.755610.

Walsh, K. (1997), Objective detection of tropical cyclones in high-resolution analyses, *Mon. Wea. Rev.*, *125*, 1767–1779.

Walsh, K. J. E., S. J. Camargo, G. A. Vecchi, A. S. Daloz, J. Elsner, K. Emanuel, M. Horn, Y.-K. Lim, M. Roberts, C. Patricola, E. Scoccimarro, A. Sobel, S. Strazzo, G. Villarini, M. W. M. Zhao, J. Kossin, T. LaRow, K. Oouchi, S. Schubert, H. Wang, J. Bacmeister, P. Chang, F. Chauvin, C. Jablonowski, H. Murakami, T. Ose, K. A. Reed, R. Saravanan, Y. Yamada, C. M. Zarzycki, P. L. Vidale, J. A. Jonas, and N. Henderson (2015), Hurricanes and climate: the U.S. CLIVAR working group on hurricanes, *Bull. Amer. Meteor. Soc.*, *96*, 997–1017, doi:10.1175/BAMS-D-13-00242.1.

Walsh, K. J. E., J. L. McBride, P. J. Klotzbach, S. Balachandran, S. J. Camargo, G. Holland, T. R. Knutson, J. P. Kossin, T.-C. Lee, A. Sobel, and M. Sugi (2016), Tropical cyclones and climate change, *WIREs Clim. Change*, *7*, 65–89, doi:10.1002/wcc.371.

Walters, D., M. Best, A. Bushell, D. Copsey, J. Edwards, P. Falloon, C. Harris, A. Lock, J. Manners, C. Morcrette, M. Roberts, R. Stratton, S. Webster, J. Wilkinson, M. Willett, I. Boutle, P. Earnshaw, P. Hill, C. MacLachlan, G. Martin, W. Moufouma-Okia, M. Palmer, J. Petch, G. Rooney, A. Scaife, and K.D.Williams (2011), The Met Office Unified Model Global Atmosphere 3.0/3.1 and JULES Global Land 3.0/3.1 configurations, *Geosci. Model Dev.*, *4*, 919–941, doi:10.5194/gmd-4-919-2011.

Watanabe, M., T. Suzuki, R. O'ishi, Y. Komuro, S. Watanabe, S. Emori, T. Takemura, M. Chikira, T. Ogura, M. Sekiguchi, K. Takata, D. Yamazaki, T. Yokohata, T. Nozawa, H. Hasumi, H. Tatebe, and M. Kimoto (2010), Improved climate simulation by MIROC5: Mean states, variability, and climate sensitivity, *J. Climate*, *23*, 6312–6335, doi:10.1175/2010JCLI3679.1.

Watanabe, S., T. Hajima, K. Sudo, T. Nagashima, T. Takemura, H. Okajima, T. Nozawa, H. Kawase, M. Abe, T. Yokohata, T. Ise, H. Sato, E. Kato, K. Takata, S. Emori,

and M. Kawamiya (2011), MIROC-ESM 2010: Model description and basic results of CMIP5-20c3m experiments, *Geosci. Model Dev. Discuss.*, *4*, 845–872, doi:10.5194/gmd-4-845-2011.

Wehner, M., Prabhat, K. A. Reed, D. Stone, W. D. Collins, and J. Bacmeister (2015), Resolution dependence of future tropical cyclone projections of CAM5.1 in the U.S. CLIVAR hurricane working group idealized configurations, *J. Climate*, *28*, 3905–3925, doi:10.1175/JCLI-D-14-00311.1.

Wehner, M. F., K. Reed, F. Li, Prabhat, J. Bacmeister, C.-T. Chen, C. Paciorek, P. Gleckler, K. Sperber, W. D. Collins, A. Gettelman, C. Jablonowski, and C. Algieri (2014), The effect of horizontal resolution on simulation quality in the Community Atmospheric Model, CAM5.1, *J. Adv. Model. Earth Syst.*, *6*, 980–997, doi:10.1002/2013MS000276.

Wu, L., C. Chou, C.-T. Chen, R. Huang, T. R. Knutson, J. J. Sirutis, S. T. Garner, C. Kerr, C.-J. Lee, and Y.-C. Feng (2014), Simulations of the present and late-twenty-first-century western North Pacific tropical cyclone activity using a regional model, *J. Climate*, *27*, 3405–3424.

Yin, J. H. (2005), A consistent poleward shift of the storm tracks in simulations of 21st century climate, *Geophys. Res. Lett.*, *32*, L18,701, doi:10.1029/2005GL023684.

Yokoi, S., Y. N. Takayabu, and H. Murakami (2013), Attribution of projected future changes in tropical cyclone passage frequency over the western North Pacific, *J. Climate*, *26*, 4096–4111, doi:10.1175/JCLI-D-12-00218.1.

Yoshimura, J., and M. Sugi (2005), Tropical cyclone climatology in a high resolution AGCM - Impacts of SST warming and CO_2 increase, *SOLA*, *1*, 133–136, doi:10.2151/sola2005-035.

Yukimoto, S., Y. Adachi, M. Hosaka, T. Sakami, H. Yoshimura, M. Hirabara, T. Y. Tanaka, E. Shindo, H. Tsujino, M. Deushi, S. Yabu, A. Obata, H. Nakano, T. Koshiro, and A. Kitoh (2012), A new global climate model of the Meteorological Research Institute: MRI-CGCM3 - Model description and basic performance, *J. Meteor. Soc. Japan*, *90A*, 23–64, doi:10.2151/jmsj.2012-A02.

Zanchettin, D., A. Rubino, D. Matei, O. Bothe, and J. H. Jungclaus (2013), Multidecadal-to-centennial SST variability in the MPI-ESM simulation ensemble for the last millennium, *Clim. Dyn.*, *40*, 1301–1318, doi:10.1007/s00382-012-1361-9.

Zhang, L., K. B. Karnauskas, J. P. Donnelly, and K. Emanuel (2017), Response of the North Pacific tropical cyclone climatology to global warming: Application of dynamical downscaling to CMIP5 models, *J. Climate*, *30*, 1233–1243, doi:10.1175/JCLI-D-16-0496.1.

Zhang, Z. S., K. Nisancioglu, M. Bentsen, J. Tjiputra, I. Bethke, Q. Yan, B. Risebrobakken, C. Andersson, and E. Jansen (2012), Pre-industrial and mid-Pliocene simulations with NorESM-L, *Geosci. Model Dev. Discuss.*, *5*, 523–533, doi:10.5194/gmd-5-523-2012.

Zhao, M., and I. M. Held (2012), TC-Permitting GCM simulations of hurricane frequency response to sea surface temperature anomalies projected for the late-twenty-first century, *J. Climate*, pp. 2995–3009, doi:10.1175/JCLI-D-11-00313.1.

Zhao, M., I. M. Held, S.-J. Lin, and G. A. Vecchi (2009), Simulations of global hurricane climatology, interannual variability and response to global warming using a 50 km resolution GCM, *J. Climate*, *22*, 6653–6678.

Table 1. Model simulations analyzed. The HWG simulations are forced with fixed SST (climatology or climatology plus 2K) and CO_2 values (present climate or twice present climate), for the present (Control) and idealized future simulations (plus 2K, 2× CO_2, plus 2K and 2× CO_2. The CMIP5 historical and future projection RCP8.5 are coupled simulations. These simulations are described in detail in *Walsh et al.* [2015] and *Taylor et al.* [2012], respectively.

Type	Name	Abbreviation	SST	CO_2
HWG	Control	ctl	climatology	present
HWG	plus 2K	p2K	clim. + 2K	present
HWG	2×CO_2	CO2	climatology	2× present
HWG	plus 2K & 2×CO_2	p2KCO2	clim. + 2K	2× present
MRI HWG	Present	pres	present	present
MRI HWG	A1B SST	FSST	future	present
MRI HWG	A1B CO2	FCO2	present	future
MRI HWG	plus 1.83K & A1B CO2	p2KFCO2	pres. + 1.83K	future
CMIP5	Historical	hist	coupled	observed
CMIP5	RCP8.5	RCP85	coupled	8.5W by 2100

Table 2. HWG models' characteristics, references for models and tracking schemes, and number of simulation years in each scenario. Definitions: LR: Low Resolution, MR: Medium Resolution, HR: High Resolution. References: Wehner: [*Wehner et al.*, 2015]; Prabhat: *Prabhat et al.* [2012]; Rockner/Scoccimarro: *Roeckner et al.* [2003] and *Scoccimarro et al.* [2011]; Walsh: *Walsh* [1997]; LaRow: *LaRow et al.* [2008]; Vitart: *Vitart et al.* [2003]; Saha: *Saha et al.* [2014]; Zhao: *Zhao et al.* [2009]; Schmidt: *Schmidt et al.* [2014]; Camargo & Zebiak: *Camargo and Zebiak* [2002]; Walters: *Walters et al.* [2011]; HB: *Hodges* [1995] and *Bengtsson et al.* [2007a, b]; Mizuta and Murakami: *Mizuta et al.* [2012] and *Murakami et al.* [2012]; Murakami: *Murakami et al.* [2012].

Model	Name	Resolution	Reference	Tracking Scheme	# Years
CAM5.1 LR	H1L	1°	Wehner	Vitart/Prabhat	24
CAM5.1 HR	H1	0.25°	Wehner	Vitart/Prabhat	16
CMCC/ECHAM5	H2T	0.75°	Rockner/Scoccimarro	Vitart/Walsh	9
CMCC/ECHAM5	H2	0.75°	Rockner/Scoccimarro	Vitart/Zhao	9
FSU	H3	1°	LaRow	Vitart/Zhao	5
GFS	H4	1°	Saha	Vitart/Zhao	20
GISS	H5	1°	Schmidt	Camargo & Zebiak	20
HadGEM3 LR	H6L	1.87°	Walters	Hodges/Bengtsson	20
HadGEM3 MR	H6M	0.83°	Walters	Hodges/Bengtsson	20
HadGEM3 HR	H6	0.35°	Walters	Hodges/Bengtsson	10
HiRAM	H7	0.5°	Zhao	Vitart/Zhao	20
MRI	H8	1.25°	Mizuta/Murakami	Murakami	25

Table 3. List of the CMIP5 models analyzed, including references, their horizontal resolution. TCs are tracked using the Camargo-Zebiak tracking routine [*Camargo and Zebiak*, 2002], as described in *Camargo* [2013].

Model	Name	Resolution	Reference
CanESM2	M1	2.9°	*von Salzen et al.* [2013]
CCSM4	M2	1.2°	*Gent et al.* [2011]
CSIRO-Mk3.6.0	M3	1.9°	*Rotstayn et al.* [2012]
FGOALS-g2	M4	3.0°	*Bao et al.* [2013]
GFDL-CM3	M5	2.5°	*Donner et al.* [2011]
GFDL-ESM2M	M6	2.5°	*Donner et al.* [2011]
HadGEM2-ES	M7	1.9°	*Jones et al.* [2011]
INM-CM4.0	M8	2.0°	*Volodin et al.* [2010]
IPSL-CM5A-LR	M9	3.7°	*Voldoire et al.* [2013]
MIROC-ESM	M10	2.8°	*Watanabe et al.* [2011]
MIROC5	M11	1.4°	*Watanabe et al.* [2010]
MPI-ESM-LR	M12	1.9°	*Zanchettin et al.* [2013]
MRI-CGCM3	M13	1.2°	*Yukimoto et al.* [2012]
NorESM1-M	M14	2.5°	*Zhang et al.* [2012]

Table 4. Downscaled models from the HWG and CMIP5 multi-model ensembles using Emanuel's technique [*Emanuel et al.*, 2006; *Emanuel*, 2006]. The downscaled models are the same as in *Daloz et al.* [2015] and *Emanuel* [2013]. The names of the downscaled models correspond to the original model names (Tables 2 and 3).

Name	Type	Original Model
dH1	HWG	CAM5.1 LR
dH2	HWG	CMCC/ECHAM5
dH5	HWG	GISS
dH7	HWG	HiRAM
dM2	CMIP5	CCSM4
dM5	CMIP5	GFDL-CM3
dM7	CMIP5	HadGEM2-ES
dM11	CMIP5	MIROC5
dM12	CMIP5	MPI-ESM-LR
dM13	CMIP5	MRI-CGCM3

Table 5. Number of WNP storms (or tracks) in each model and scenario for the HWG multi-model ensemble. Models in boldface were selected to be used when comparing present and future climates using two criteria: number of storms available and similarity of the storm tracks by clusters with observations. In cases that more than one version of tracks were available per model type (using different model resolution or tracking scheme) only one version of the model tracks was considered. See text for more details of the selection criteria. For the explicit models, the median number of storms per year is shown in <ctl>, as well the median number of named storms per year in observations for the period 1981-2010.

Name	Type	ctl	p2K	CO2	p2kCO2	Total	<ctl>
H1L	HWG	24	29	33	29	115	1
H1	HWG	153	105	169	157	584	9
H2T	HWG	482	404	436	418	1740	48.2
H2	HWG	354	272	343	313	1282	35.4
H3	HWG	145	133	135	105	518	29.0
H4	HWG	92	80	83	80	335	3.7
H5	HWG	579	528	681	637	2425	28.9
H6L	HWG	190	175	218	–	583	8.6
H6M	HWG	138	109	119	–	366	13.8
H6	HWG	128	100	126	–	354	16
H7	HWG	677	648	591	482	2398	33.8
		pres	FSST	FCO2	p2KFCO2	Total	<ctl>
H8	HWG	747	627	528	728	2630	6.2
		ctl	p2K	CO2	p2kCO2	Total	
dH1	downs. HWG	2987	2267	2434	2184	9872	
dH2	downs. HWG	2858	2744	2764	2738	11104	
dH5	downs. HWG	2799	2979	2888	2997	11663	
dH7	downs. HWG	2575	2576	2711	2705	10567	
Observed climatology per year: 28.5							

Table 6. Number of WNP storms (or tracks) in each model and scenario for the CMIP5 multi-model ensemble. Models in boldface were selected to be used when comparing present and future climates using two criteria: number of storms available and similarity of the storm tracks by clusters with observations. See text for more details of the selection criteria. For the explicit models, the median number of storms per year is shown in <hist>, as well the median number of named storms per year in observations for the period 1981-2010.

		hist	RCP85	Total	<hist>
M1	CMIP5	346	443	789	17.3
M2	CMIP5	62	144	206	3.1
M3	CMIP5	1009	1568	2577	50.4
M4	CMIP5	252	140	392	12.6
M5	CMIP5	697	903	1600	34.8
M6	CMIP5	1520	1258	2778	76.0
M7	CMIP5	255	344	599	12.7
M8	CMIP5	13	111	124	0.6
M9	CMIP5	85	297	382	4.2
M10	CMIP5	27	16	43	1.3
M11	CMIP5	354	402	756	17.7
M12	CMIP5	974	991	1965	48.7
M13	CMIP5	2330	832	3162	116.5
M14	CMIP5	20	31	51	1.0
		hist	RCP85	Total	
dM2	downs. CMIP5	10413	18241	28654	
dM5	downs. CMIP5	8748	14966	23714	
dM7	downs. CMIP5	7332	13641	20973	
dM10	downs. CMIP5	7006	11950	18956	
dM11	downs. CMIP5	9004	14808	23812	
dM12	downs. CMIP5	7253	13064	20317	
Observed climatology per year: 28.5					

Table 7. Statistical significant changes (0.1 level) in variance in Y in future scenarios with a northward (N) shift, compared with the present climate in the recurving clusters A, C, E and G. Future scenarios p2K, CO2, p2KCO2, RCP85 are indicated as 1, 2, 3 and 4 in the table.

Model	A	C	E	G
H1	1N 2N 3N	1N	2N	
H2		1N 2N 3N	2N	
H3	1N 2N			1N
H4	1N 2N 3N	1N 2N 3N	1N 2N	1N 3N
H5			2N	1N
H6	1N 2N		1N	1N
H7	3N			3N
dH1				2N 3N
dH2	1N	3N		
M1		4N		
M2				4N
M3	4N		4N	
M7				4N
M11	4N		4N	
M12		4N	4N	
dM2	4N			
dM5	4N		4N	
dM7	4N			
dM12	4N			4N

Table 8. Statistical significant changes (0.1 level) in centroid X, variance of X and lifespan in future scenarios compared with the present climate in cluster F. Variance of X and lifespan are labeled B for bigger and S for smaller. Centroid of X is labeled E for East and W for West. Also shown in the table with a $\star$ are the models for which cluster F could not be identified.

Model	Variance X	Lifespan	Model	Centroid X	Lifespan
H1	1S 2S 3S	1S 2S 3S	M1		4S
H2	1S 2S 3S	1S 3S	M2	4E	4B
H3	3S	1B 2S 3S	M11	4E	4S
H5	1S 3S		M12	4E	
H6	1B 2B	1B 2B	dM2	4E	
H7	1B 2B	1S 2S 3S	dM5	4W	4S
H8	1S 2S 3B	2S 3B	dM7	4E	4B
dH1	2S		dM11	4W	
dH5		1S 3S	dM12		4S
			dM13	4W	4S
H4	$\star$	$\star$	M7	$\star$	$\star$

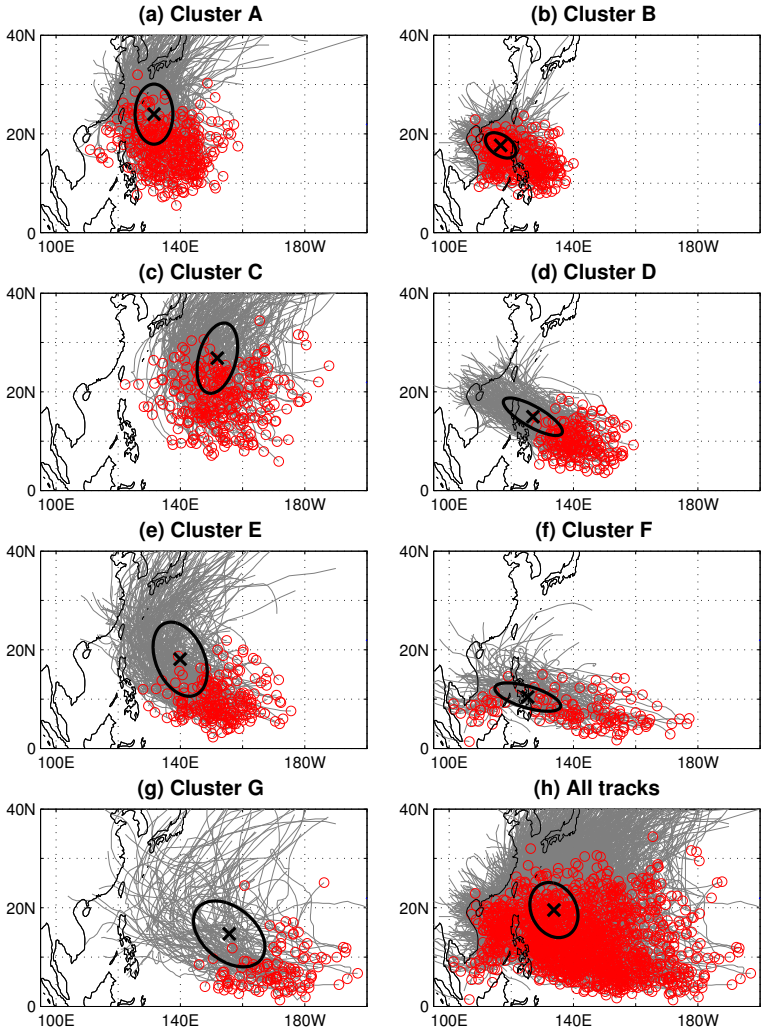

Figure 1: Western North Pacific observed tracks for the period 1950-2013. Panels (a) to (g) show the tracks (in grey) in individual clusters based in the classification of *Camargo et al.* [2007a,b]. The initial positions are marked in red circles. The mean mass moments ellipses are shown in black, with the centroids marked with a black x.

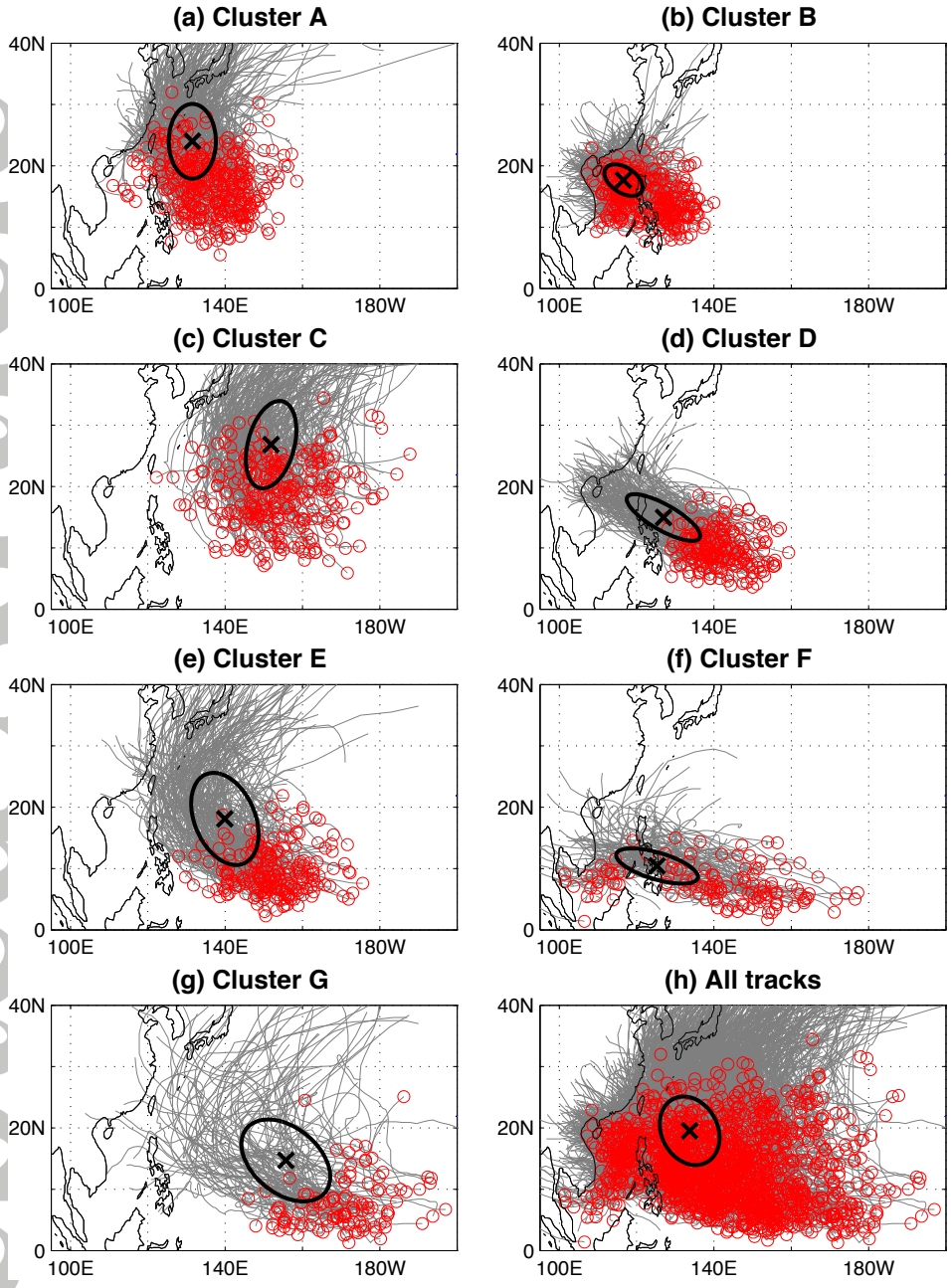

Figure 1. Western North Pacific model tracks (grey), genesis (red circles) and mass moments ellipses and centroids (black) for the current climate in selected models. The left panels show tracks from the explicit models, the right panels the corresponding downscaled models. HWG (CMIP5) models are shown in panels (a) and (c) ((e) and (g)) in the control (historical) simulations. Two hundred randomly selected tracks are shown in each panel.

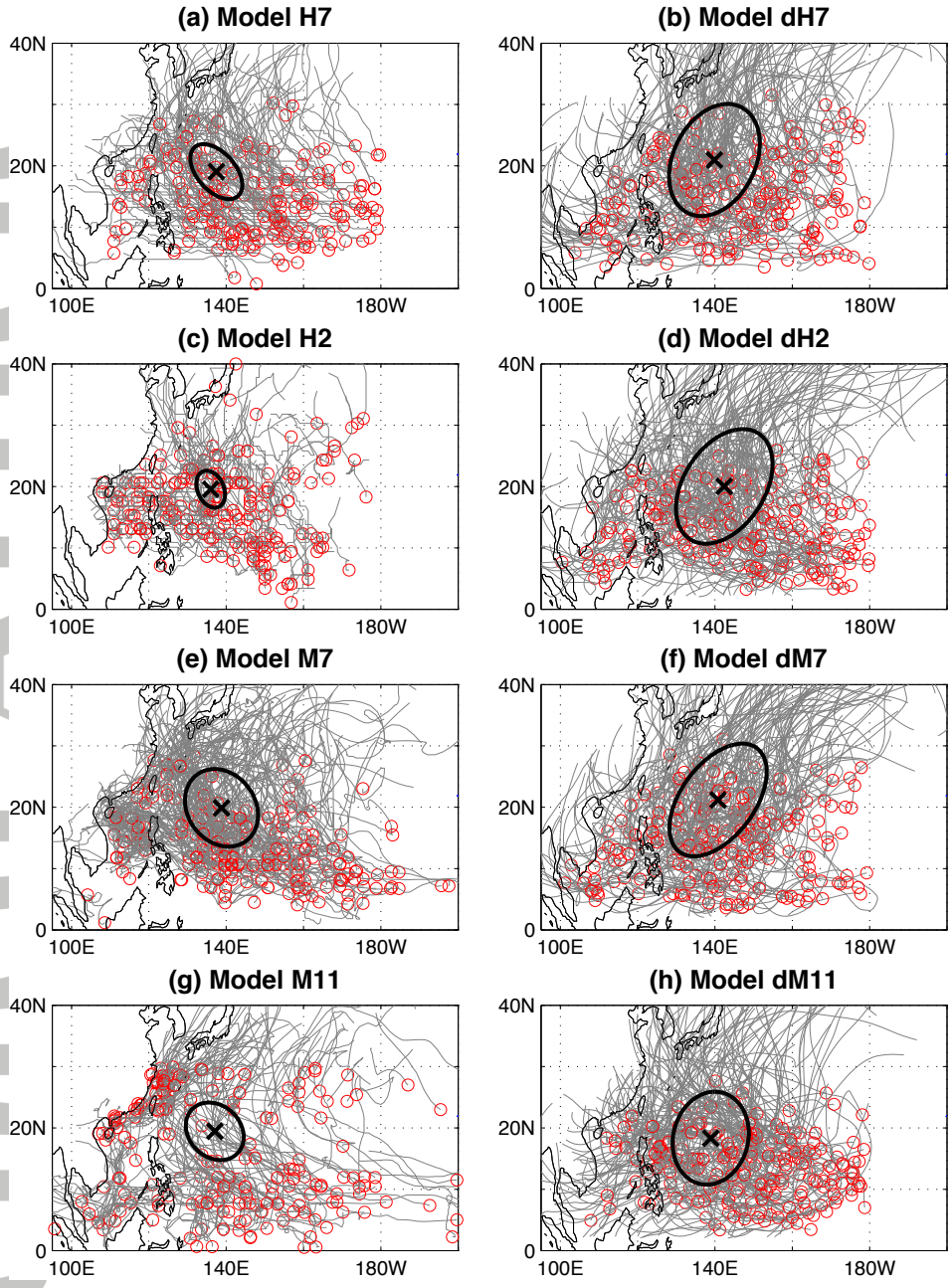

Figure 2. Western North Pacific mass moment ellipses for the current climate in all models. The left panels show the ellipses from the explicit models, the right panels from the downscaled models.

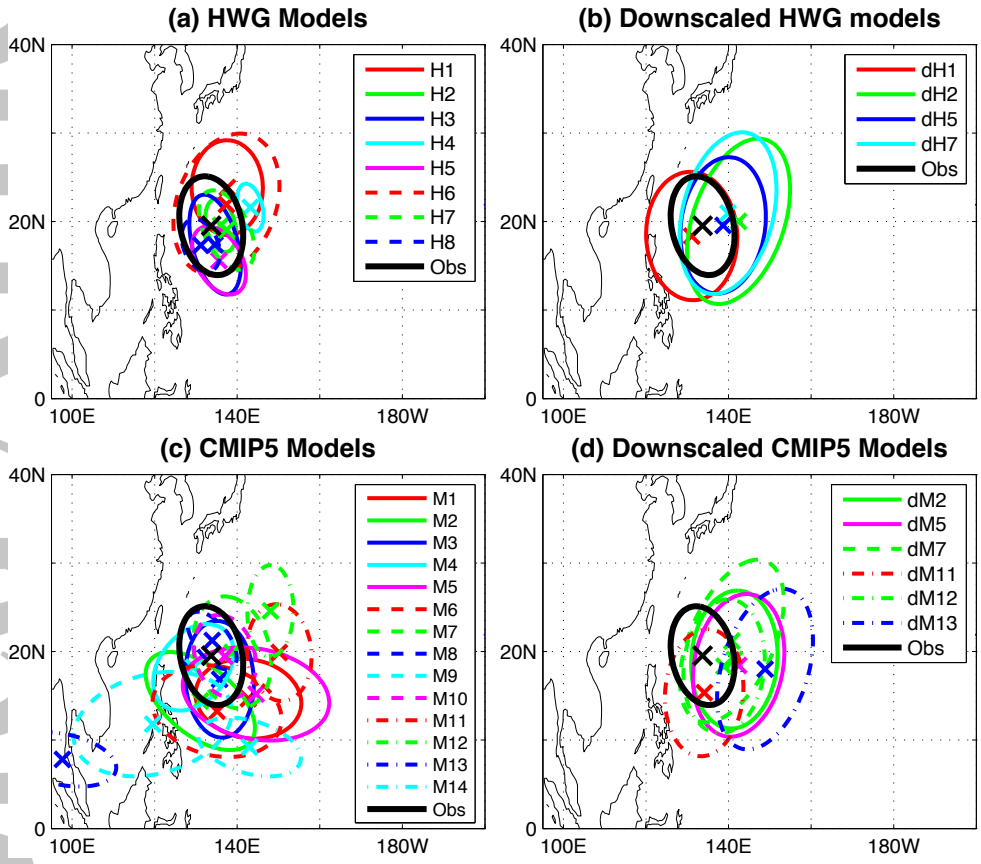

Figure 3. Western North Pacific model tracks in individual clusters for CMIP5 model M12 in the historical simulation. Model clusters that do not correspond to any of the observed clusters are marked with an asterisk (∗).

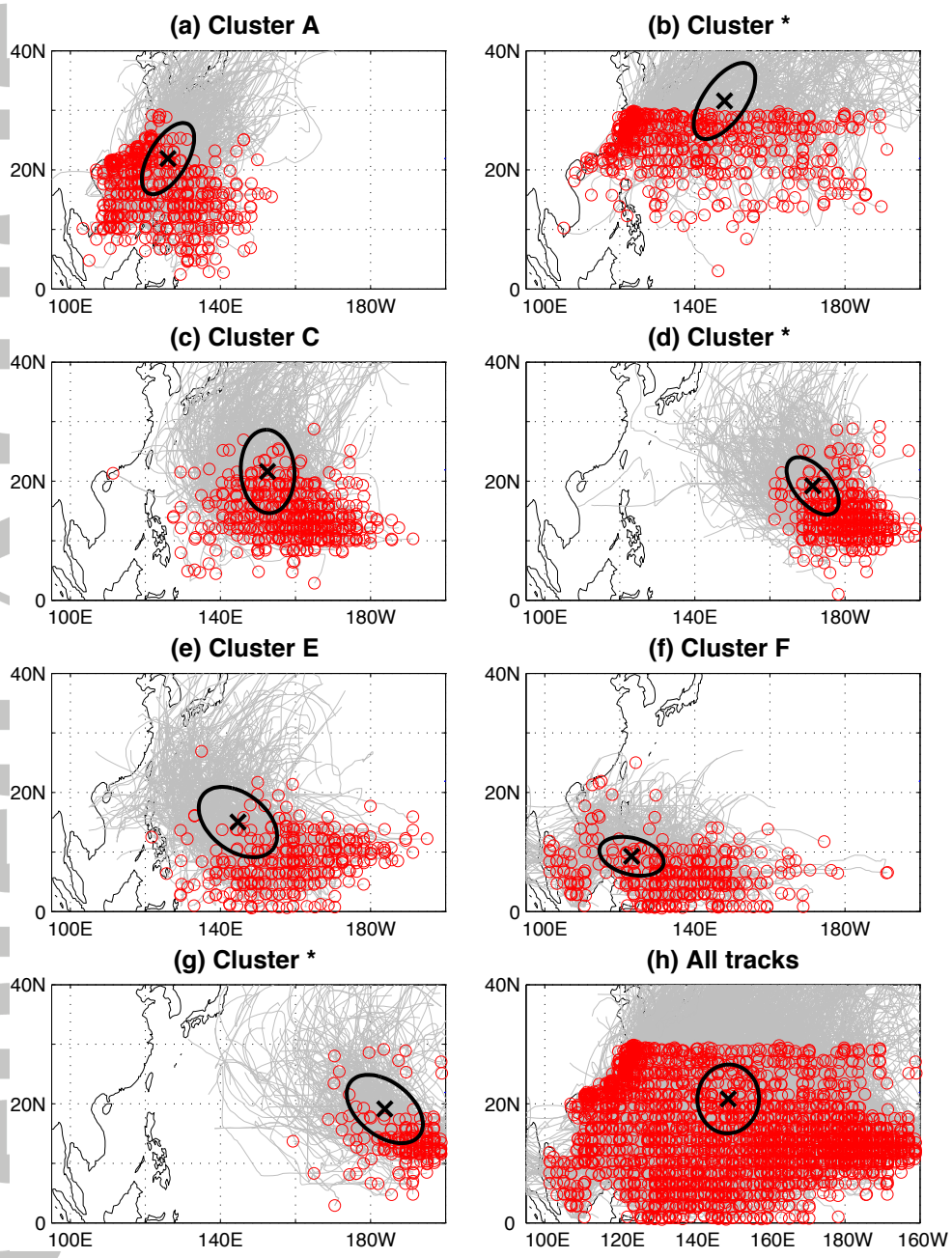

Figure 4. Western North Pacific model tracks in individual clusters for HWG model H7 in the present climate simulation. Two hundred randomly selected tracks are shown in each panel.

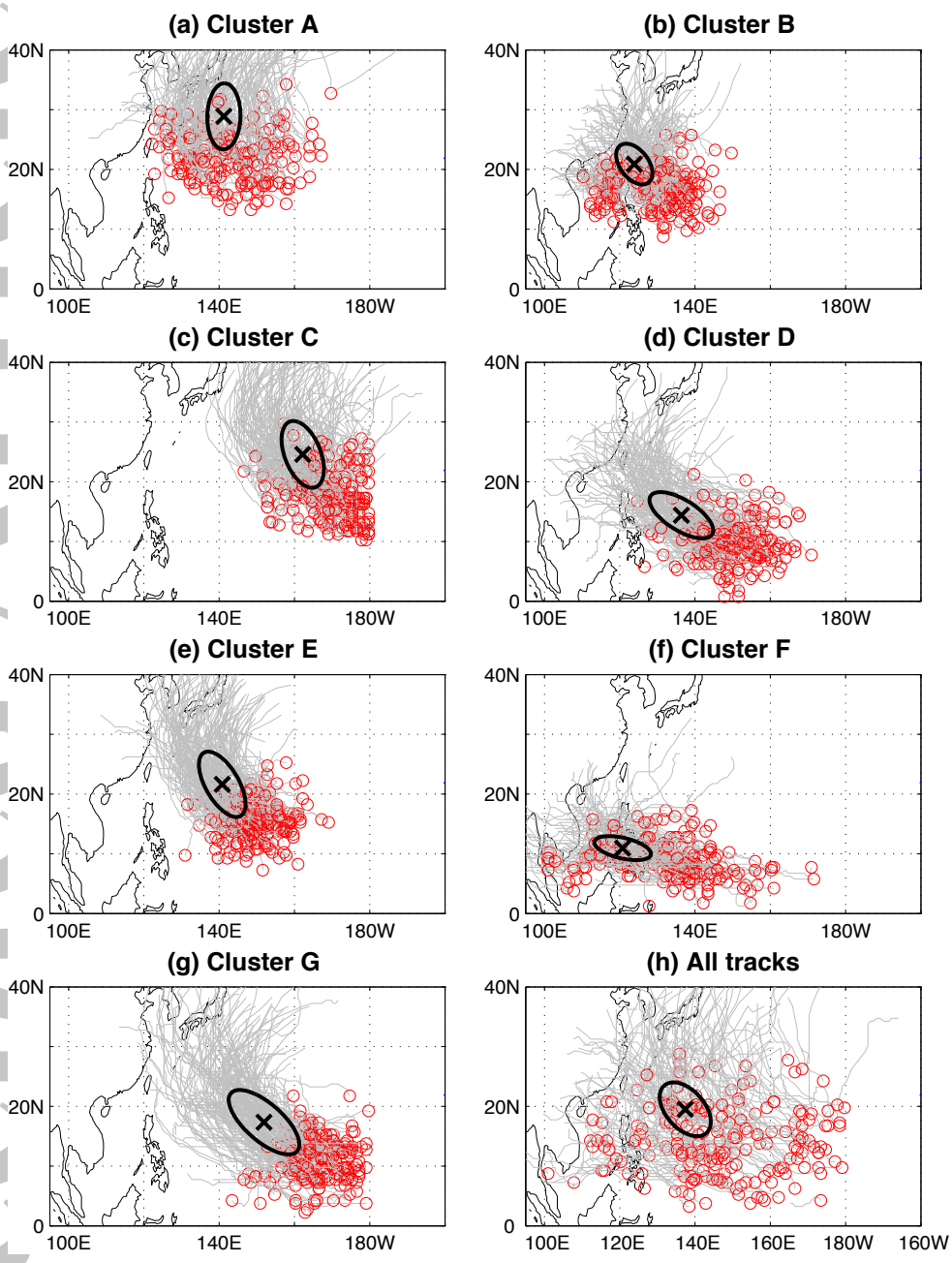

Figure 5. Western North Pacific model tracks in individual clusters for the downscaled CMIP5 model dM12 in the present climate simulation. Two hundred tracks are shown in each panel.

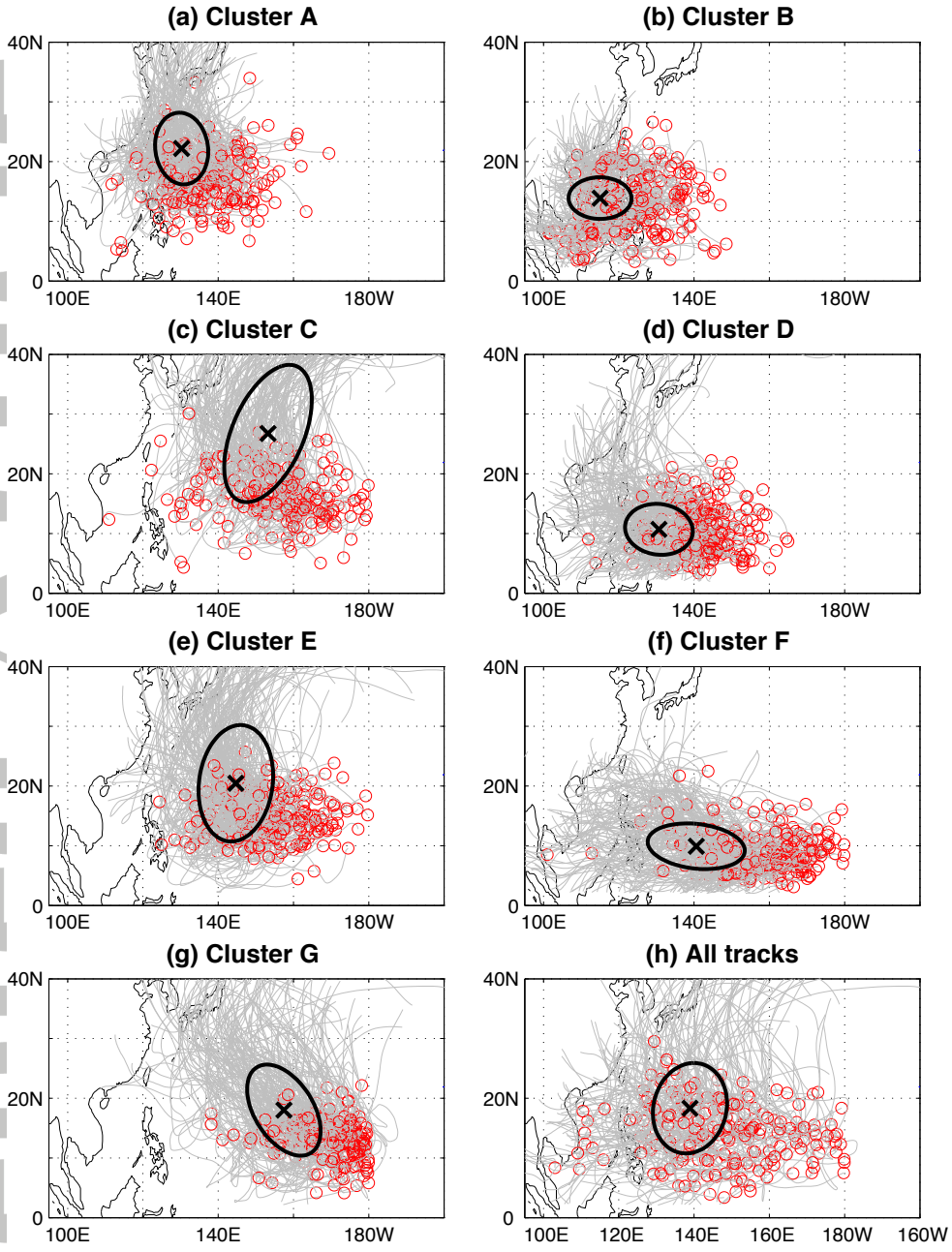

Figure 6. Percentage of storms assigned to each cluster per model and scenario for the HWG explicit tracks. Clusters not corresponding to observed clusters are marked with a star. None of the models showed a statistically significant change in the cluster assignment occurrence in future climates.

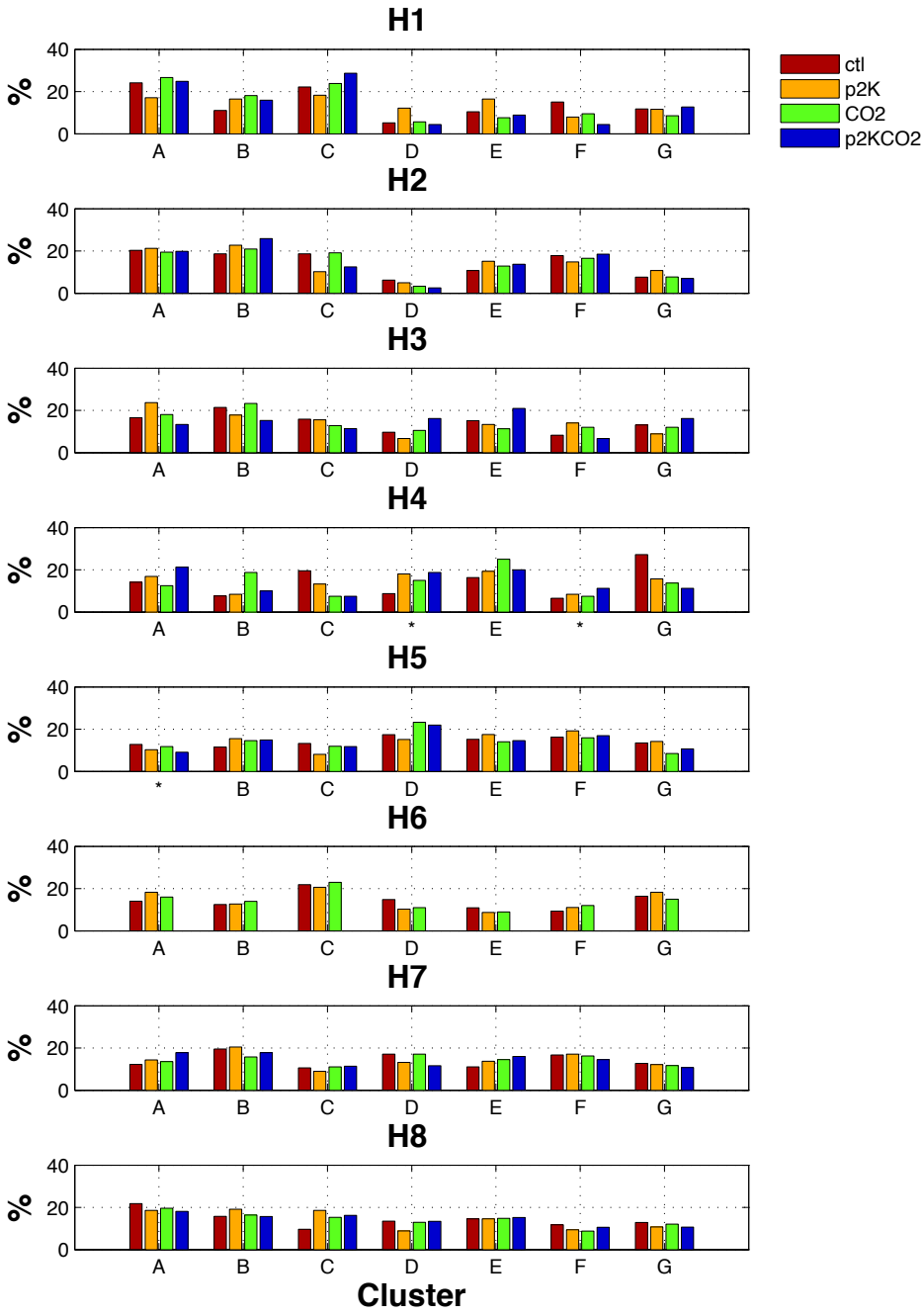

Figure 7. Kernel smoothed centroid X probability distributions estimates (PDE) as function of longitude for (i) cluster E for ctl and CO2 scenarios for selected HWG models (panels (a)-(f)); (ii) cluster F for hist and RCP85 scenarios for selected CMIP5 and downscaled CMIP5 models (panels (g)-(l)). The vertical lines mark the median in each probability distribution.

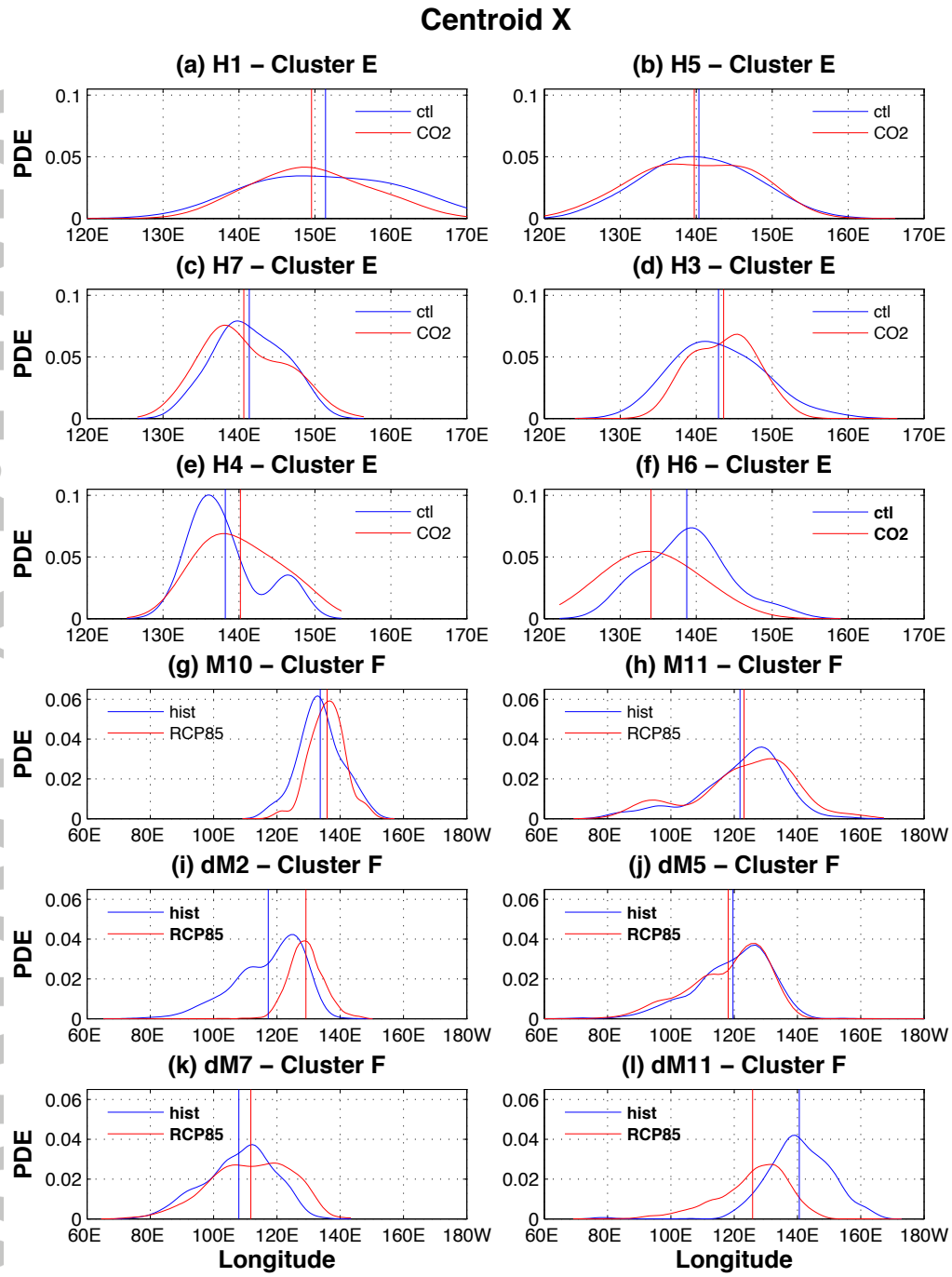

Figure 8. Track ellipses in cluster A for selected models that have a statistically significant increase in the variance of Y, for HWG (panels (a)-(d)) and CMIP5 models (panels (e)-(j)).